# INTERPRETATION OF STRONG-MOTION EARTHQUAKE ACCELEROGRAMS: THE BEAR VALLEY EVENT OF 1973

Lawrence S. Turnbull, Jr., et al

Texas Instruments, Incorporated
Dallas, Texas

30 June 1974

ALEX(02)-FR-74-01

AD-785 419

# INTERPRETATION OF STRONG-MOTION EARTHQUAKE ACCELEROGRAMS: THE BEAR VALLEY EVENT OF 1973

**FINAL REPORT**

**1 MAY 1972 TO 1 MAY 1974**

Prepared by
Lawrence S. Turnbull, Jr., and James C. Battis

TEXAS INSTRUMENTS INCORPORATED
Equipment Group
Post Office Box 6015
Dallas, Texas 75222

Contract No. F44620-72-C-0073
Amount of Contract: $98,994
Beginning 1 May 1972
Ending 30 April 1974

Prepared for

AIR FORCE OFFICE OF SCIENTIFIC RESEARCH

Sponsored by

ADVANCED RESEARCH PROJECTS AGENCY
Nuclear Monitoring Research Office
ARPA Program Code No. 2F10
ARPA Order No. 2134

30 June 1974

Acknowledgment: This research was supported by the Advanced Research Projects Agency, Nuclear Monitoring Research Office, under Project VELA-UNIFORM, and accomplished under the direction of the Air Force Office of Scientific Research under Contract No. F44620-72-C-0073.

UNCLASSIFIED

SECURITY CLASSIFICATION OF THIS PAGE (When Data Entered)

| REPORT DOCUMENTATION PAGE | READ INSTRUCTIONS BEFORE COMPLETING FORM |
|---|---|
| 1. REPORT NUMBER: AFOSR - TR - 74 - 1437 | 2. GOVT ACCESSION NO. / 3. RECIPIENT'S CATALOG NUMBER |
| 4. TITLE (and Subtitle): INTERPRETATION OF STRONG-MOTION EARTHQUAKE ACCELEROGRAMS: THE BEAR VALLEY EVENT OF 1973 | 5. TYPE OF REPORT & PERIOD COVERED: Final |
| | 6. PERFORMING ORG. REPORT NUMBER: ALEX(02)-FR-74-01 |
| 7. AUTHOR(s): Lawrence S. Turnbull, Jr., and James C. Battis | 8. CONTRACT OR GRANT NUMBER(s): F44620-72-C-0073 |
| 9. PERFORMING ORGANIZATION NAME AND ADDRESS: Texas Instruments Incorporated, Equipment Group, Dallas, Texas 75222 | 10. PROGRAM ELEMENT, PROJECT, TASK AREA & WORK UNIT NUMBERS: ARPA Program Code No. 2F10 |
| 11. CONTROLLING OFFICE NAME AND ADDRESS: Advanced Research Projects Agency, Nuclear Monitoring Research Office, Arlington, Virginia 22209 | 12. REPORT DATE: 30 June 1974 |
| | 13. NUMBER OF PAGES: 67 |
| 14. MONITORING AGENCY NAME & ADDRESS (if different from Controlling Office): Air Force Office of Scientific Research, 1400 Wilson Boulevard, Arlington, Virginia 22209 | 15. SECURITY CLASS. (of this report): UNCLASSIFIED |
| | 15a. DECLASSIFICATION/DOWNGRADING SCHEDULE |

16. DISTRIBUTION STATEMENT (of this Report)

APPROVED FOR PUBLIC RELEASE, DISTRIBUTION UNLIMITED

17. DISTRIBUTION STATEMENT (of the abstract entered in Block 20, if different from Report)

18. SUPPLEMENTARY NOTES

ARPA Order No. 2134



19. KEY WORDS (Continue on reverse side if necessary and identify by block number)

Near-Field Earthquake Strong-Motion Records
Dislocation Modeling of Near-Field Motion
Stick-Slip
Non-Planar Fault Surface
Spectral Analysis

20. ABSTRACT (Continue on reverse side if necessary and identify by block number)

The solutions to eight earthquakes have been obtained from near-field strong-motion accelerograms using Haskell's moving dislocation source model. In particular, the solutions to the San Fernando main shock and three small aftershocks were re-examined using the corrected orientation of the Pacoima Dam instruments. A reasonable match to the observed waveforms for the main event could only be obtained by having

DD FORM 1 JAN 73 1473 EDITION OF 1 NOV 65 IS OBSOLETE

UNCLASSIFIED

SECURITY CLASSIFICATION OF THIS PAGE (When Data Entered)

20. continued

a large strike-slip dislocation component on the deeper segments of the fault. Also, new locations and orientations were obtained for the three small aftershocks.

Using botn Haskell's model and spectral analysis, the Bear Valley earthquake of June 22, 1973 was examined. Both approaches yielded substantially the same results; a large dislocation on the order of 100 cm over a small fault area of less than 1.0 $km^2$, with a seismic moment ($M_o$) of 1.2 to 1.5 x $10^{25}$ dyne-cm. This value of the seismic moment appears large to those of the other events when plotted versus local magnitude ($M_L$); the other seven events generally follow a linear log moment-magnitude relation.

## ABSTRACT

The solutions to eight earthquakes have been obtained from near-field strong-motion accelerograms using Haskell's moving dislocation source model. In particular, the solutions to the San Fernando main shock and three small aftershocks were re-examined using the corrected orientation of the Pacoima Dam instruments. A reasonable match to the observed waveforms for the main event could only be obtained by having a large strike-slip dislocation component on the deeper segments of the fault. Also, new locations and orientations were obtained for the three small aftershocks.

Using both Haskell's model and spectral analysis, the Bear Valley earthquake of June 22, 1973 was examined. Both approaches yielded substantially the same results; a large dislocation on the order of 100 cm over a small fault area of less than 1.0 $km^2$, with a seismic moment ($M_o$) of 1.2 to 1.5 x $10^{25}$ dyne-cm. This value of the seismic moment appears large to those of the other events when plotted versus local magnitude ($M_L$); the other seven events generally follow a linear log moment-magnitude relation.

TABLE OF CONTENTS

LIST OF FIGURES

LIST OF FIGURES
(continued)

LIST OF FIGURES
(continued)

LIST OF FIGURES
(continued)

LIST OF TABLES

# SECTION I
# INTRODUCTION

For the past two years, we have applied Haskell's moving dislocation source model in the interpretation of near-field strong-motion earthquake records. This work, begun by Ben Tsai and Howard Patton, has continued for the past year with the objectives to (1) throughly determine the limitations of the source model and the validity of any complexity added to it, and (2) to apply the model to recent events which were recorded on strong-motion instruments. In this report, we will present a brief summary of the results given in previous technical reports, present our revised analysis of the San Fernando earthquake, and our interpretation of the Bear Valley earthquake of June 22, 1973.

The summary of the previous results is given in Section II. We review the software development, and the selection of the source-time function for the model. A brief description of Tsai and Patton's solution for the San Fernando earthquake and its first aftershock, the Parkfield earthquake, and the Borrego Mountain earthquake is also given. Finally, our analysis of the San Fernando earthquake using a segmented fault with varying rupture velocities is presented.

After the research had been completed for the last technical report (Turnbull and Battis, 1973), it was determined that the horizontal components at the Pacoima Dam site, which recorded the San Fernando earthquake, were aligned incorrectly. This resulted in a $30^{o}$ error in the direction of the instruments. Using this new alignment, the main shock and three small aftershocks are re-analyzed in Section III.

Because the mechanism of the San Fernando earthquake was mainly dip-slip, the Bear Valley event of June 22, 1973 offered an opportunity to analyze a different mechanism (mainly strike-slip). Three solutions are presented in Section IV using the Haskell model, and they are then compared to fault parameters obtained from spectral analysis.

Finally, in Section V, we summarize our results and indicate the direction these studies will take in relation to future source mechanism investigations.

# SECTION II

# HASKELL'S DISLOCATION MODEL APPLIED TO SEVERAL EARTHQUAKES

During the initial stages of this investigation, Tsai and Patton (1972) established much of the software and the technical approachs inherent in them. Major programs were written which calculated and displayed theoretical waveforms from the Haskell model (see Appendix A). A unified format was established for storing strong-motion records on nine-track magnetic tape. In processing these records, it was found that a linear and a cubic least squares corrections of the acceleration and the integrated velocity waveform, respectively, resulted in reasonably reliable experimental velocity waveforms. These one-time integrated velocity waveforms were found to be far less sensitive to various schemes of numerical integration and baseline corrections than the corresponding twice integrated displacement waveforms. Therefore, the comparison of the experimental and the theoretical waveforms is carried out at the velocity level.

In this comparison, Tsai and Patton (1972) found that a linear ramp dislocation source-time function appeared to be superior to an exponential ramp function in the generation of the theoretical waveforms. Using the velocity traces obtained from accelerograms recorded at the Pacoima Dam site during the San Fernando earthquake of February 9, 1971, theoretical waveforms were generated with both source time functions and matched to this observed data. The exponential velocity function proved to be inferior in both the quality of the theoretical velocity waveforms and in the source parameters obtained from the 'best' match. A linear ramp velocity function has been used in the analysis of all earthquakes in this study.

Having established competent theoretical model software and a uniform data format two events were initially analyzed by Tsai and Patton (1972). Interpretation of the accelerograms at the Pacoima Dam site recorded during the San Fernando earthquake of February 9, 1971 yielded the picture of rupture initiating at the depth level of the instrumentally-determined focus and then propagating up and to the south, past and under the accelerograph site along a fault surface dipping at $52^{\circ}$. The final dislocation was estimated to be 150 cm, with a rise time of 0.6 sec, and a seismic moment of $10.4 \times 10^{25}$ dyne-cm. From their analysis of the Parkfield earthquake of June 28, 1966, as recorded at Station 2, the motion was found to be right-lateral strike-slip with a dislocation of 200 cm along a 10 km segment of the San Andreas fault near Station 2. The dislocation began at a point northwest of the recording site and propagated past the southeast of Station 2. The dislocation rise time was estimated to be 0.9 sec, with a seismic moment of $1.8 \times 10^{25}$ dyne-cm. Tsai and Patton's estimates, when compared with other seismological observations, suggest that the dislocation associated with the Parkfield earthquake is not uniform over the whole fault length of up to 37 km, but concentrated along the 10 km segment near the southeastern end of the fault.

After further study, Tsai and Patton (1973) re-examined these two events, which resulted in slight modifications. For the San Fernando earthquake, the final dislocation was found to be 120 cm with the seismic moment $8.3 \times 10^{25}$ dyne-cm. This latter number is comparable to the one determined from surface wave data by Canitez and Toksoz (1972), $7.5 \times 10^{25}$ dyne-cm. Re-examination of the Parkfield earthquake yielded a fault length 15 km and the relatively low rupture velocity of 2.2 cm/sec.

In this same study, Tsai and Patton (1973) analyzed the first aftershock of the San Fernando earthquake as recorded at Pacoima Dam and the Borrego Mountain earthquake of April 9, 1968. For the aftershock, they

divided the main event fault plane into forty-five segments and attempted to obtain a unique match from one of these segments. One solution was judged better than the rest, although its uniqueness was not conclusively proved. This solution, located near the southwest corner of the main event fault plane, yielded a rise time of 0.1 sec, a velocity of rupture of 3.0 km/sec, with a pure thrust dislocation motion of 12 cm and seismic moment of $4.7 \times 10^{23}$ dyne-cm. This latter value, by comparison, was 1/175 of that of the main shock.

Analysis of the Borrego Mountain Earthquake did not yield a unique solution. Two modes of rupture, one unilateral, the other bilateral, could not be distinguished from the data on hand. From the unilateral rupture solution, a rise time of 0.8 sec with a final dislocation of 100 cm was obtained. For a fault 32 km long by 20 km wide, the seismic moment was $1.9 \times 10^{26}$ dyne-cm. In both solutions, the model was assumed to be vertical right lateral strike-slip.

One of the most important results from the analysis of these four events was that the Haskell model is limited to data obtained from recording accelerographs located within a few kilometers of the fault trace. This is due to the lack of the model accounting for a half space, layering, and propagation effects. Another important result from the analysis of these four events concerned the need for a finite rupture velocity. For the San Fernando earthquake, the Parkfield earthquake, and the Borrego Mountain earthquake, a dislocation model with a finite rupture velocity is required to explain the observed near-field velocity waveforms. An instantaneous dislocation model for these earthquakes is unacceptable. As for the first San Fernando aftershock, the choice between a finite moving dislocation and an instantaneous dislocation model is inconclusive, probably because of the small fault area.

Continuing with the work of Tsai and Patton, Turnbull and Battis (1973) analyzed the San Fernando earthquake and three of its aftershocks recorded on strong-motion instruments at Pacoima Dam using different source model geometric configurations. It was found that, without independent estimates of the fault parameters, the credibility of the solutions obtained from the fitting procedure using the Haskell moving dislocation model is drastically reduced. Although we can use a least squares technique to fit the dislocation amplitude, the interrelationships of the fault orientation, fault dimensions, rupture velocity, and rise time make our solution highly non-unique. If strong-motion records having good azimuthal coverage and good quality accelerograms are available, reasonable estimates of fault length, rupture velocity, near-field corner frequencies, and rise time can be obtained.

When the source model is generalized to include segments having their own rupture velocities, dislocations, and dimensions, the effect of stick-slip (segmented rupture velocities) is not major within a moderate range of rupture velocities. But having two segments with different dip angles (a hinged fault surface), significant changes do occur. In particular, the initial negative trend in the vertical S-wave trace of the main shock recorded at Pacoima Dam can be matched using fault geometry which includes a hinged surface.

In this same study, solutions were given for the San Fernando earthquake with a hinged surface and for three small aftershocks. Since that report, it was determined that the horizontal components at the Pacoima Dam site were aligned incorrectly, which resulted in a $30^{o}$ error in the direction of the instruments. The corrected solution is given in the next section.

## SECTION III

## REVISED SOLUTIONS TO THE SAN FERNANDO EARTHQUAKE AND THREE AFTERSHOCKS

The original solution with a hinged fault surface, and with the incorrect alignment of the instruments, was given by Turnbull and Battis (1973). The correct alignment of the horizontal components was then found to be N75W and S15W instead of S74W and S16E, respectively. The fit of the theoretical velocity waveform to the observed waveform recorded at Pacoima Dam is shown in Figure III-1. Again, as in the previous solution, a poor fit of the amplitude of the vertical component occurs, but the pulse width and shape on all components is noticeably better.

A cross-section of the theoretical model which generated these theoretical waveforms is shown in Figure III-2. The changes in the dip angles, from $33^{\circ}$ to $60^{\circ}$ in the old solution to $30^{\circ}$ and $65^{\circ}$ in the new solution, seem quite small, but are essential to produce the negative initial trends of the N75$^{\circ}$W and down components.

The parameters describing each segment of the fault are listed in Table III-1. The most significant changes occur in the direction and magnitude of the dislocations, especially on the lower element. A reasonable match to the observed waveforms could only be accomplished by having a large strike-slip component on this segment of the fault. We also found that the upper segments were mainly dip-slip, and did not have as great an affect as the lower segments. These results agree with the study by Alewine (1974), especially in terms of the large dislocations on the lower segments of the fault.

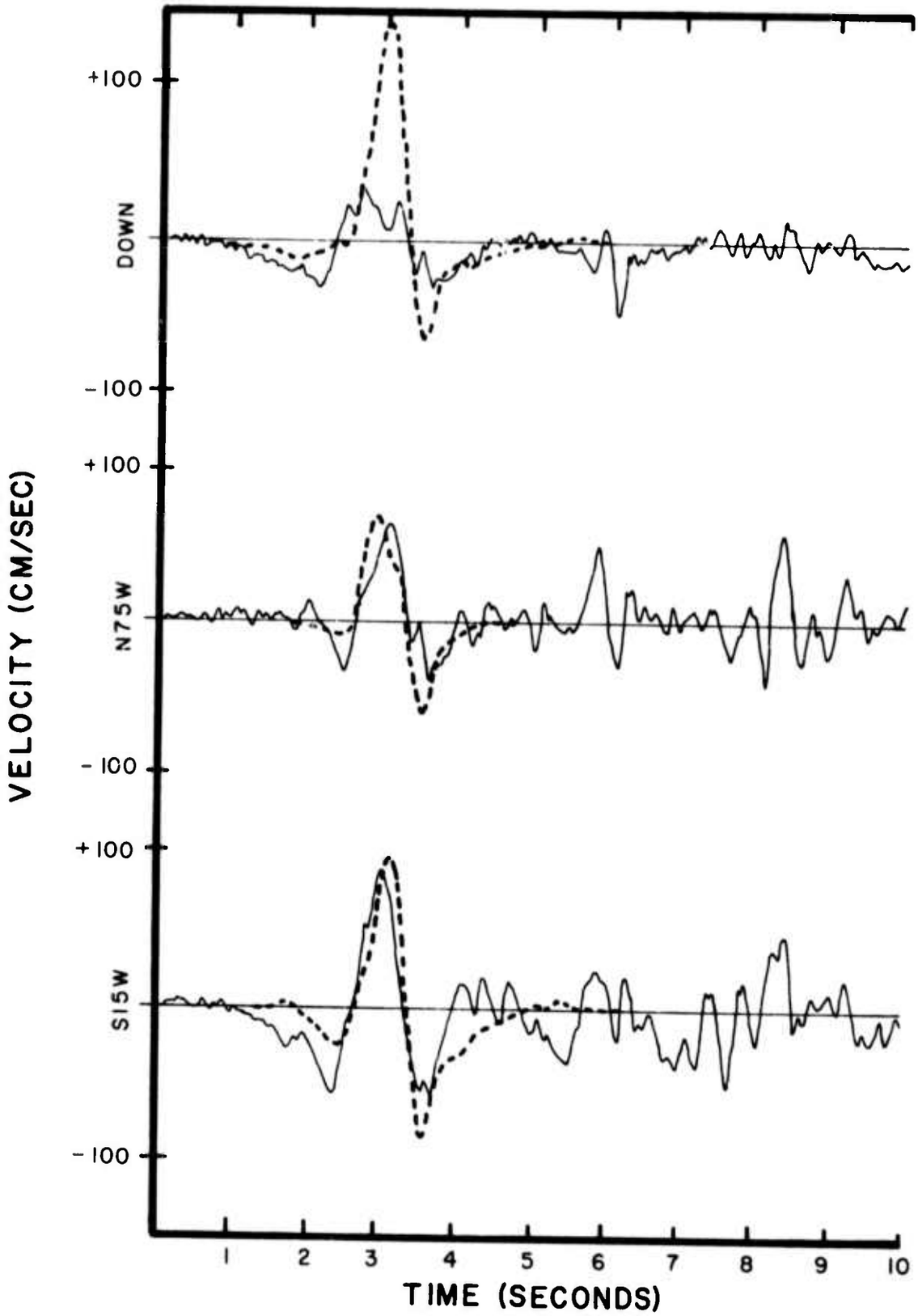


FIGURE III-1

OBSERVED (SOLID CURVE) AND THEORETICAL (DASHED CURVE) VELOCITY WAVEFORM OF THE SAN FERNANDO EARTHQUAKE AS RECORDED AT PACOIMA DAM

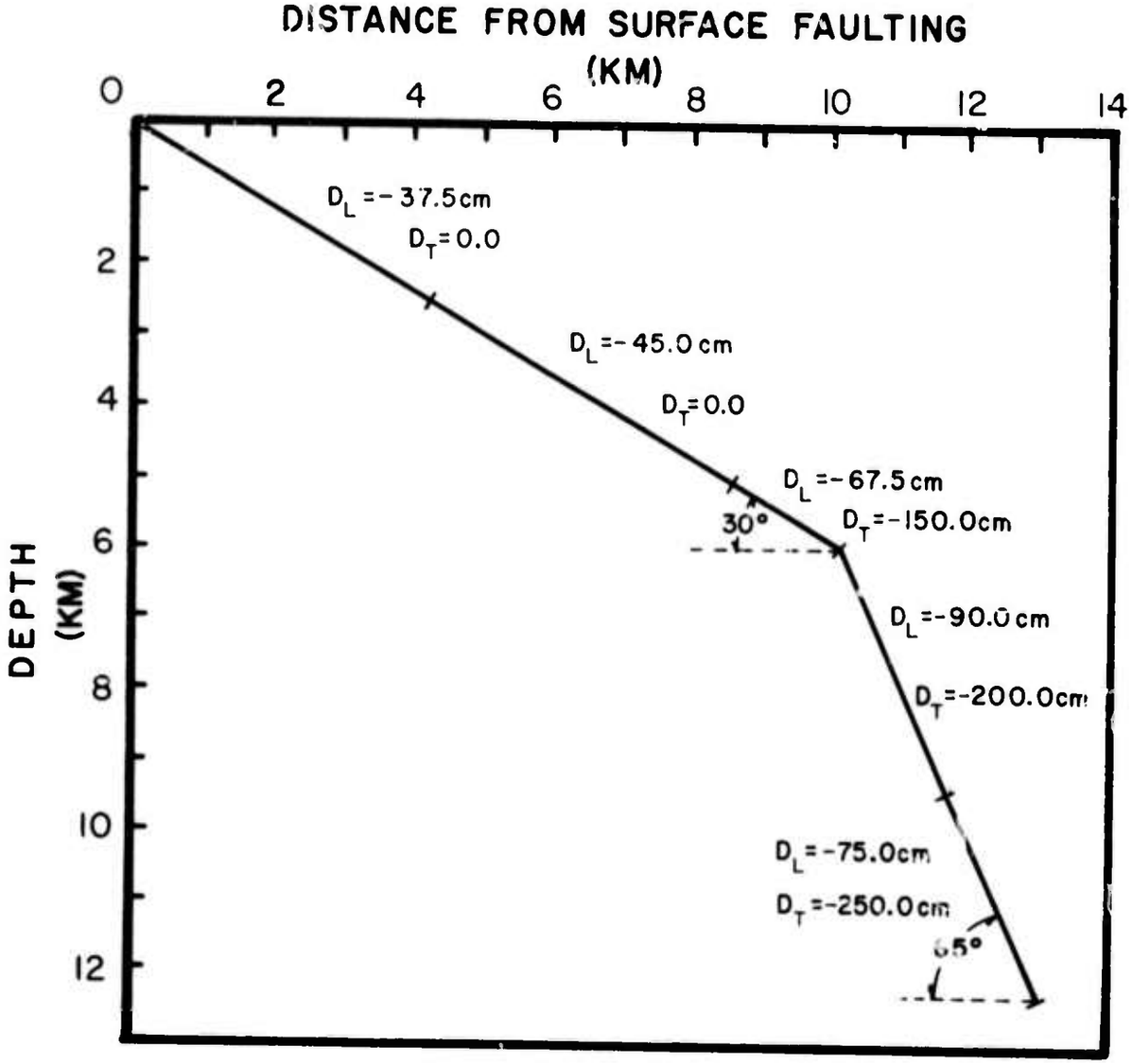


FIGURE III-2

CROSS SECTION OF SAN FERNANDO EARTHQUAKE
FAULT SURFACE

TABLE III-1

SAN FERNANDO EARTHQUAKE
FAULT PARAMETERS

Hypocenter: X = 9.18 km
Y = 6.00 km
Z = -12.24 km

Strike: N70W

Constants: $V_p$ = 5.5 km/sec $V_s$ = 3.2 km/sec

Moment: $M_o = 9.6 \times 10^{25}$ Dyne-cm

Segment 1

Width = 12.0 km
Rise Time = 0.6 sec
Dip = 65°
$D_L$ = -75.0 cm
Length = 3.5 km
Rupture Velocity = 3.0 km/sec
$D_T$ = -250.0 cm

Segment 2

Width = 14.0 km
Rise Time = 0.6 sec
Dip = 65°
$D_L$ = -90.0 cm
Length = 3.5 km
Rupture Velocity = 2.88 km/sec
$D_T$ = -200.0 cm

Segment 3

Width = 16.0 km
Rise Time = 0.6 sec
Dip = 30°
$D_L$ = -67.5 cm
Length = 1.8 km
Rupture Velocity = 2.95 km/sec
$D_T$ = -150.0 cm

Segment 4

Width = 14.0 km
Rise Time = 0.3 sec
Dip = 30°
$D_L$ = -45.0 cm
Length = 5.0 km
Rupture Velocity = 3.0 km/sec
$D_T$ = 0.0

Segment 5

Width = 12.0 km
Rise Time = 0.15 sec
Dip = 30°
$D_L$ = -37.5 km
Length = 5.0 km
Rupture Velocity = 3.2 km/sec
$D_T$ = 0.0

We also re-examined the three small aftershocks previously analyzed. In Figure III-3, a comparison of this study's location estimates with those of Trifunac's (1972) are shown. Events 4 and 11 show the same locations from the two investigations, while the estimates of the location of event 30 differ. The solutions presented here should not be considered the only correct solutions, but the best possible within the limitations of the model.

A summary of the fault parameters used in the solutions of these aftershocks is given in Table III-2. The differences from the previous solutions are only in the source coordinates and the fault orientations (strike angle). Unlike the main shock, the hypocentral location, fault dimensions, and fault orientation of these events do not have independent estimates.

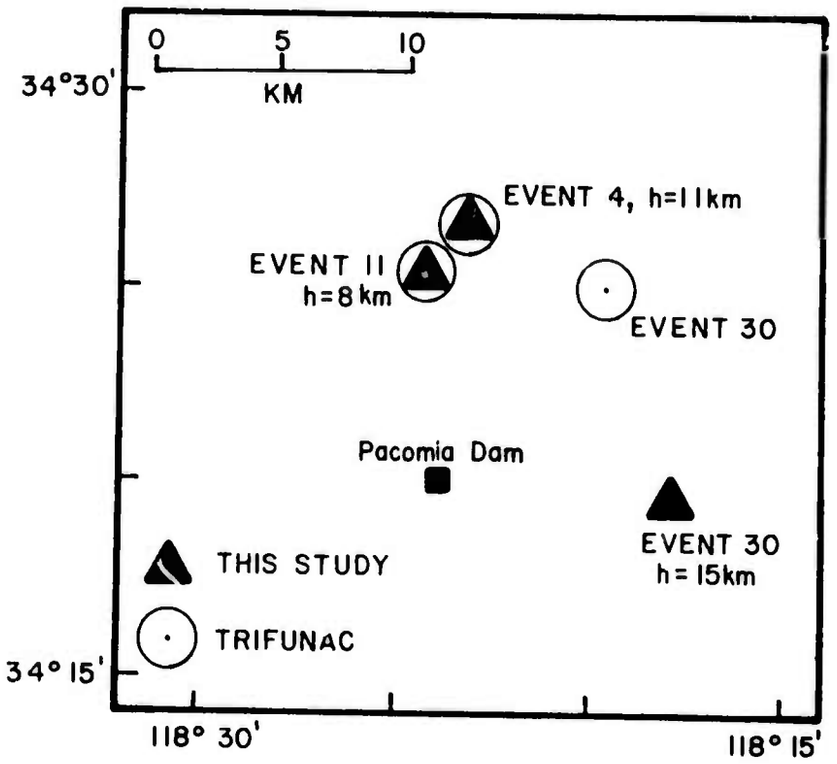


FIGURE III-3

AFTERSHOCKS OF THE SAN FERNANDO EARTHQUAKE, LOCATIONS BY TRIFUNAC (OPEN CIRCLES) AND LOCATIONS BY DISLOCATION MODEL (TRIANGLES)

TABLE III-2

AFTERSHOCKS OF THE SAN FERNANDO EARTHQUAKE - FEBRUARY 9, 1973

| | | Event 4 | Event 11 | Event 30 |
|---|---|---|---|---|
| $V_P$ (km/sec) | | 5.5 | 5.5 | 5.5 |
| $V_S$ (km/sec) | | 3.2 | 3.2 | 3.2 |
| Width (km) | | 1.0 | 1.0 | 0.75 |
| Length (km) | | 1.0 | 1.0 | 1.0 |
| Rise Time (sec) | | 0.03 | 0.03 | 0.025 |
| Rupture Velocity (km/sec) | | 3.0 | 3.0 | 3.15 |
| Dip Angle | | 80° | 80° | 52° |
| Strike Angle | | N80W | N80W | N70W |
| Source Coordinates (Relative to Pacoima Dam/km) | X | 7.84 | 5.0 | 5.0 |
| | Y | -5.72 | -6.35 | 7.0 |
| | Z | -11.0 | -8.08 | -15.0 |
| Longitudinal Dislocation | | -8.37 | -40.69 | -3.02 |
| Transverse Dislocation (cm) | | -0.41 | -0.46 | -0.45 |
| Seismic Moment (Dyne·cm) | | $26.3 \times 10^{21}$ | $123.5 \times 10^{21}$ | $7.8 \times 10^{21}$ |
| Local Magnitude | | 4.3 | 4.7 | 4.0 |

## SECTION IV

## THE BEAR VALLEY EARTHQUAKE OF JUNE 22, 1973

On June 22, 1973 a relatively deep, low magnitude earthquake occurred at Bear Valley, California (approximately 30 km southeast of Hollister), and in the immediate vicinity of a well instrumented segment of the San Andreas Fault. Due to the proximity of the epicenter to the University of California eight station accelerometer array, this event had the potential for providing a unique opportunity to investigate the source characteristics of a low magnitude earthquake. The significance of this event, as compared to the previously studied San Fernando earthquake aftershock sequence, lies not only in the difference in mechanism (dip-slip in the case of the aftershocks while strike-slip for the Bear Valley event), but also in the availability of restrictions on the solution. In contrast to the aftershock sequence, which were recorded only in the very near-field with usable signals at Pacoima Dam, a sufficient number of intermediate-field records were obtained to allow accurate hypocentral location and fault plane solutions. These, when coupled with the near-field coverage, greatly reduce the non-uniqueness inherent in the Haskell moving dislocation model.

In the vicinity of Bear Valley, the San Andreas Fault divides the crustal structure into two distinct blocks, a high velocity, granitic and metamorphic structure to the southwest and lower velocity sedimentaries on the northeast side of the fault. Using different crustal velocity structures to represent this velocity contrast across the fault, two different epicenters have been calculated(Figure IV-1). Epicenter E-1, approximately 0.5 km north and 1 km west of station 2 was determined using a velocity model

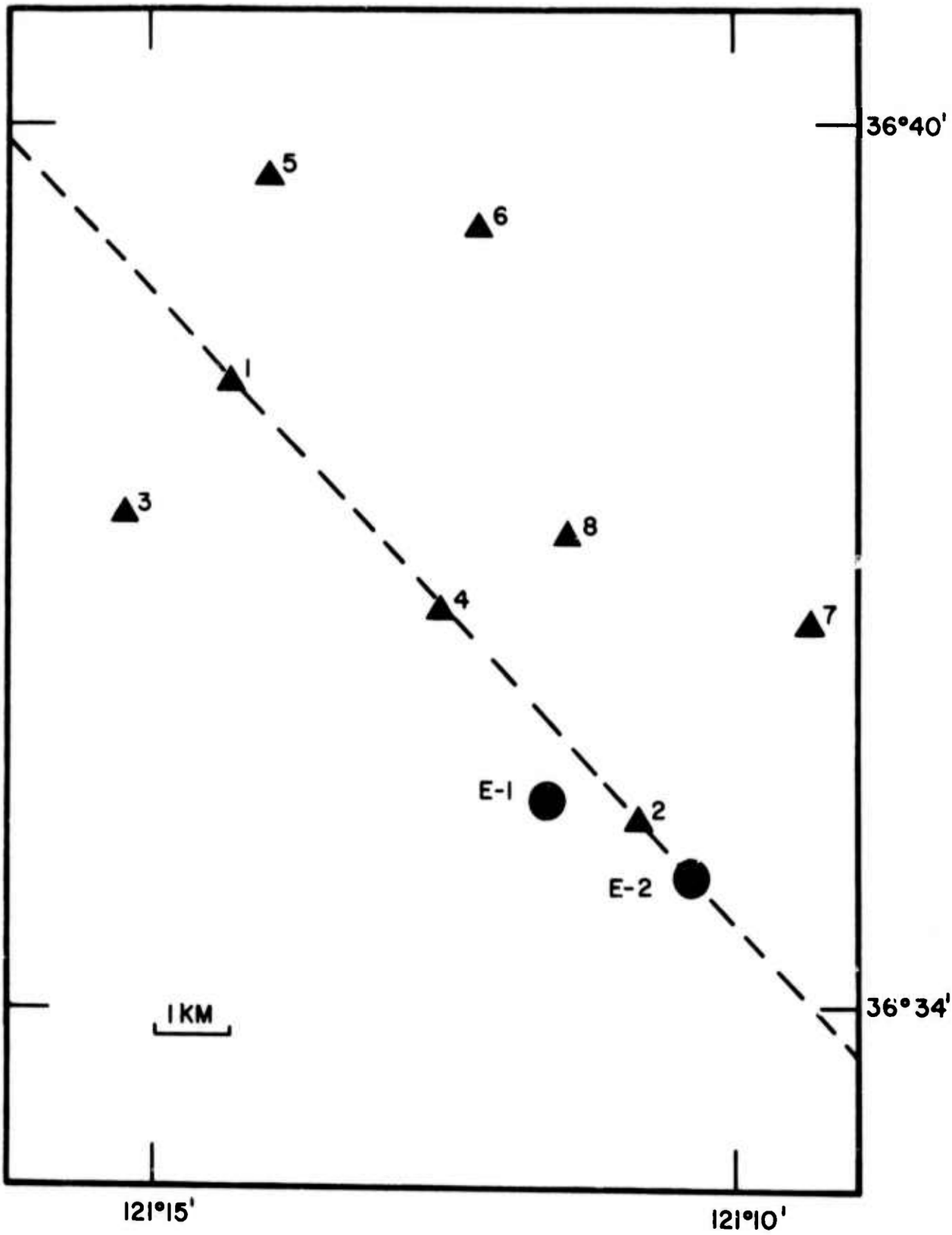


FIGURE IV-1

MAP LOCATING TWO EPICENTERS (CIRCLES) OF THE BEAR VALLEY EARTHQUAKE AND THE ACCELEROMETER ARRAY RECORDING THE EVENT

representing an average structure across the San Andreas Fault. When the velocity contrast is incorporated into the location scheme, a second epicenter, E-2, is found (Johnson, personal communication). In both cases, a depth of approximately 10 km is assigned to the event. A solution for the source parameters of the earthquake was obtained at each epicenter to evaluate the significance of the epicentral change with respect to the Haskell model.

Based on data from separate arrays, two fault plane solutions have also been obtained for this event. These two solutions, one by Berkeley and the other by the University of Washington, are in general agreement (Malone, personal communication), with strike angles of N39$^{o}$W and N41$^{o}$W, respectively. The associated dip angles are less accurately determined, but are in the range of 70$^{o}$ to 80$^{o}$, dipping to the northwest.

The accelerometer array which recorded the Bear Valley Earthquake is in the rough form of a rectangle lying parallel to the surface trace of the San Andreas Fault (Figure IV-1). Stations 1, 2, and 4 lie directly on the fault, Station 3 is on the higher velocity structure of the southwestern sedimentary structure. In the study of this earthquake, the complex geology of the region and the unusual depth of the event essentially restrict analysis to the southeastern stations of the array, Stations 2, 4, 7, and 8. Waveforms at the more distant stations are probably effected by transmission and site effects which can not be duplicated by the model.

Our analysis will be presented in two parts. The first involves the usual procedure of generating theoretical waveforms and determining the 'best' fit solution of the observed data. The second involves spectral analysis of the accelerogram, using approximations by Brune (1970) to determine fault parameters. Comparisons of fault parameter estimates from the two methods of analysis are presented.

## A. APPLICATION OF THE HASKELL DISLOCATION SOURCE TO THE BEAR VALLEY EARTHQUAKE

### 1. Methods of Solution

Identical methods were used in searching for restricted solutions (in terms of strike direction and dip angle) at both epicenters. Using a vertical fault with a strike direction of N40$^{o}$W, the fault length, width, rupture velocity and rise time were adjusted to fit the pulse width of the empirical velocity wave at Station 8. At each epicenter, theoretical waveforms for transverse and longitudinal dislocations were evaluated at Station 8 for strike directions between N45$^{o}$W and N35$^{o}$W, with rupture occurring either to the northwest or southeast. In addition, the dip angle was varied for each strike direction between 60$^{o}$ and 90$^{o}$. A least-squares error combination of the two dislocations was calculated to fit the Station 8 empirical waveform. The parameters of this fit were then used to produce theoretical waveforms at Stations 2, 4, and 7. The parameters which produced the best fit of the empirical data were then determined by inspection. Due to the poor signal quality of Stations 2 and 4, the evaluation of the theoretical results at these stations were made on the basis of signal amplitudes rather than strict waveform fitting.

Essentially the same method was used in obtaining an unrestricted (in terms of strike direction and dip angle) solution. In this case, the strike and dip angles were not limited in range. Least-squares error fits were obtained at Station 8 for 5$^{o}$ increments over the entire sweep of 360$^{o}$ in strike angle, using a vertical fault. The dip angle was then changed by 5$^{o}$ and the strike angles around the minimum residual for the previous case were searched for a minima at the new dip angle. This process is continued until a change in dip angle increases the residual of the fit at Station 8 implying a local minima has been found. Four such local minima were found for epicenter E-1. A comparison of the predicted waveforms at

Stations 2, 4, and 7 were then made for each set of parameters and the best fit was determined, again by inspection.

2. Solutions for the Restricted and Unrestricted Cases

Three solutions have been found for the Bear Valley Earthquake. One at each epicenter, based on the restrictions of the fault plane solutions and a third, at epicenter E-1, where no restrictions were placed on the solution (Tables IV-1, IV-2, IV-3).

The fault dimensions, rupture velocity and rise time are identical in each case. These parameters are not independent, as together they control the pulse width and the complexity of the theoretical waveform. In the case of the Bear Valley Earthquake, it may be shown that values which diverge to any significant degree from the listed values (for example, an increase in the fault dimensions), produce waveforms too complex or of too long duration to match the Bear Valley accelerograms (Appendix B).

In terms of waveform fitting, the restricted solutions at each epicenter (Figures IV-2 and IV-3) are essentially identical, duplicating the empirical waveforms equally well. For both cases, the S-wave at Station 8 (Figures IV-2a, IV-3a) is well fitted, which should be expected, as it is the station which was used in the least squares fitting. As was previously stated, the velocity wave traces at Stations 2 (Figures IV-2b, IV-3b) and 4 (Figures IV-2c, IV-3c) were only used as limiting factors on the amplitudes of these stations. The theoretical traces over estimate the amplitudes at these stations, but not to an important degree. It should be noted that the Haskell model cannot predict accurate arrival times, as the model assumes the fault surface to lie within a whole-space. Assuming that the arrival time at Station 8 is correct, a shift of less than 0.2 seconds was required to match theoretical and observed pulses at Station 7. Identification of the S-phase at Stations 2 and 4 are virtually impossible and the theoretical waves were compared to

TABLE IV-1

BEAR VALLEY EARTHQUAKE - JUNE 22, 1973
RESTRICTED SOLUTION - EPICENTER E-1

| | |
|---|---|
| Epicenter: | $36^{o}$ 35.4'N |
| | $121^{o}$ 11.6'W |
| Depth: | 10.5 km |
| Velocities: | $V_p$ = 5.5 km/sec |
| | $V_s$ = 3.2 km/sec |
| Strike: | N40W |
| Dip: | $75^{o}$ to NE |
| Fault Dimensions: | L = 0.5 km |
| | W = 0.75 km |
| Rise Time: | 0.1 sec |
| Rupture Velocity: | 3.1 km/sec |
| Dislocations: | Strike-Slip: 100 cm |
| | Dip-Slip : 42 cm |
| Moment: | $1.2 \times 10^{23}$ dyne-cm |

TABLE IV-2

BEAR VALLEY EARTHQUAKE - JUNE 22, 1973
RESTRICTED SOLUTION - EPICENTER E-2

| | |
|---|---|
| Epicenter: | $36^{o}$ 34.9'N |
| | $121^{o}$ 10.4'W |
| Depth: | 10.5 km |
| Velocities: | $V_p$ = 5.5 km/sec |
| | $V_s$ = 3.2 km/sec |
| Strike: | N40$^{o}$W |
| Dip: | $75^{o}$ to NE |
| Fault Dimensions: | L = 0.5 km |
| | W = 0.75 km |
| Rise Time: | 0.1 sec |
| Rupture Velocity: | 3.1 km/sec |
| Dislocations: | Strike-Slip: 100 cm |
| | Dip-Slip : 0 cm |
| Moment: | $1.2 \times 10^{23}$ dyne-cm |

TABLE IV-3

BEAR VALLEY EARTHQUAKE - JUNE 22, 1973
UNRESTRICTED SOLUTION - EPICENTER E-1

| | |
|---|---|
| Epicenter: | $36^{\circ}$ 35.4'N<br>$121^{\circ}$ 11.6'W |
| Depth: | 9.5 km |
| Velocities: | $V_p$ = 5.5 km/sec<br>$V_s$ = 3.2 km/sec |
| Strike: | N47.5$^{\circ}$W |
| Dip: | $80^{\circ}$ to SW |
| Fault Dimensions: | L = 0.5 km<br>W = 0.75 km |
| Rise Time: | 0.1 sec |
| Rupture Velocity: | 3.1 km/sec |
| Dislocations: | Strike-Slip: 250 cm<br>Dip-Slip : 0 cm |
| Moment: | $2.8 \times 10^{23}$ dyne-cm |

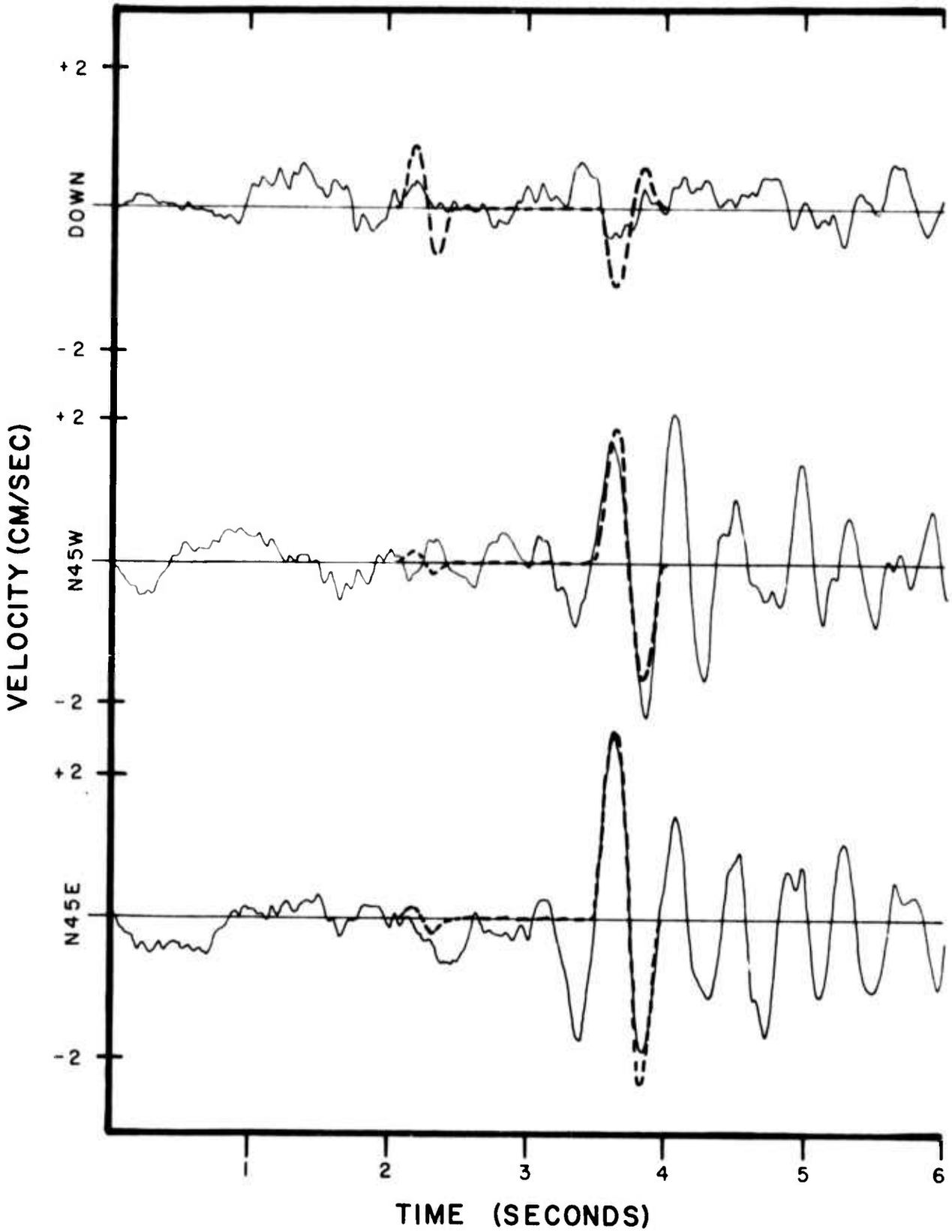


FIGURE IV-2a

OBSERVED (SOLID CURVE) AND THEORETICAL (DASHED CURVE) VELOCITY TRACE FOR RESTRICTED SOLUTION OF BEAR VALLEY EARTHQUAKE AT EPICENTER E-1, SITE 8

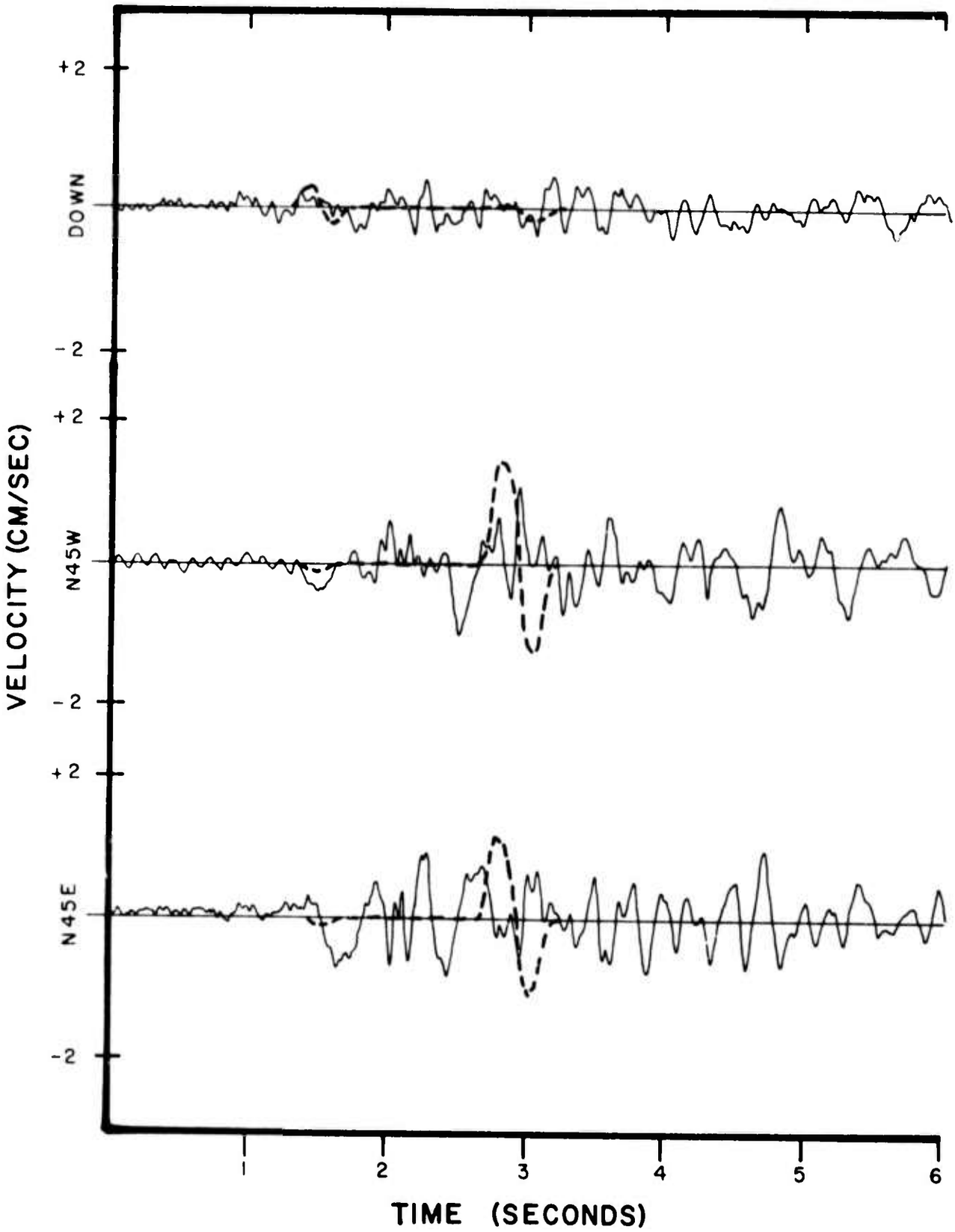


FIGURE IV-2b

OBSERVED (SOLID CURVE) AND THEORETICAL (DASHED CURVE) VELOCITY TRACE FOR RESTRICTED SOLUTION OF BEAR VALLEY EARTHQUAKE AT EPICENTER E-1, SITE 2

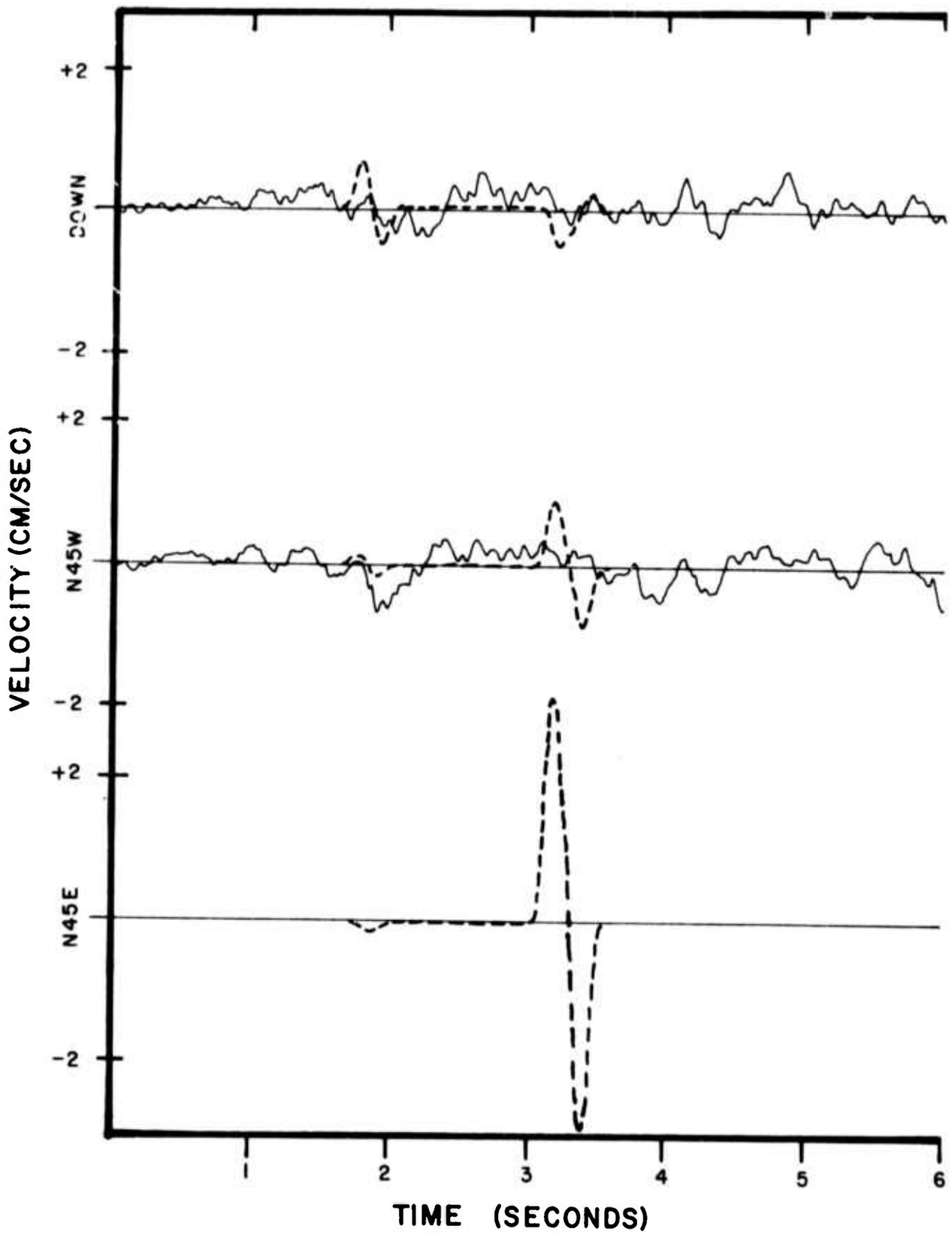


FIGURE IV-2c

OBSERVED (SOLID CURVE) AND THEORETICAL (DASHED CURVE) VELOCITY TRACE FOR RESTRICTED SOLUTION OF BEAR VALLEY EARTHQUAKE AT EPICENTER E-1, SITE 4

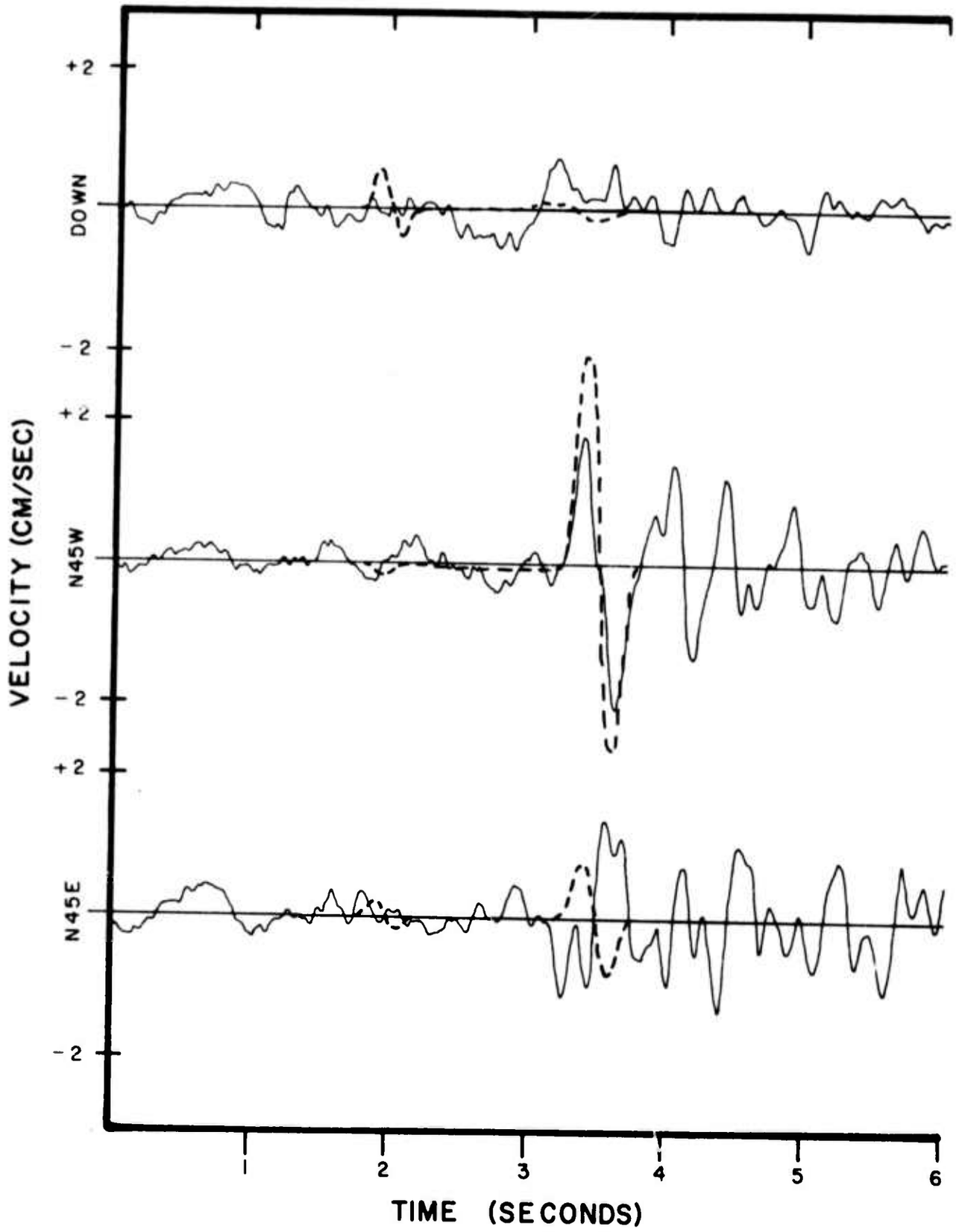


FIGURE IV-2d

OBSERVED (SOLID CURVE) AND THEORETICAL (DASHED CURVE) VELOCITY TRACE FOR RESTRICTED SOLUTION OF BEAR VALLEY EARTHQUAKE AT EPICENTER E-1, SITE 7

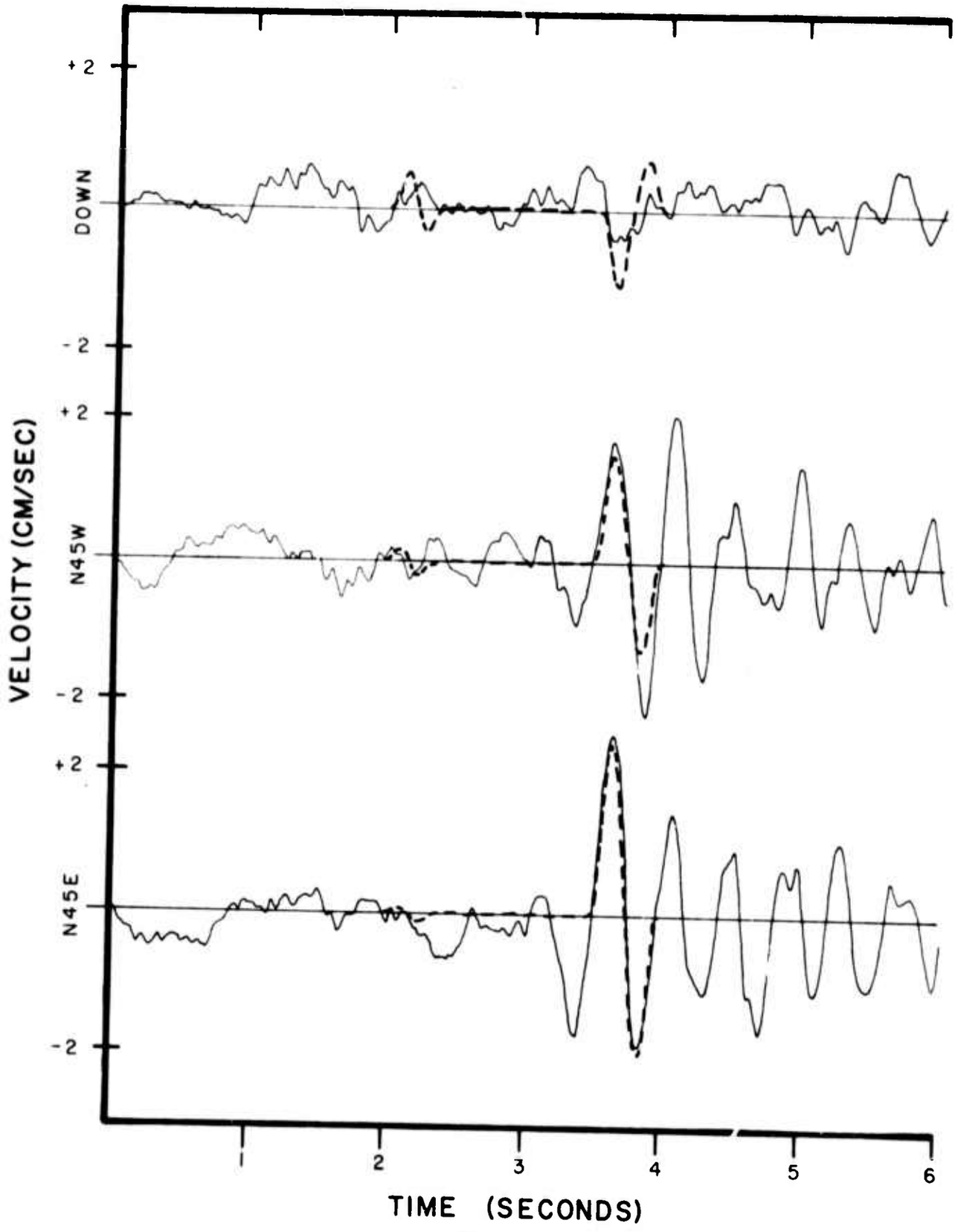


FIGURE IV-3a

OBSERVED (SOLID CURVE) AND THEORETICAL (DASHED CURVE) VELOCITY TRACE FOR RESTRICTED SOLUTION OF BEAR VALLEY EARTHQUAKE AT EPICENTER E-2, SITE 8

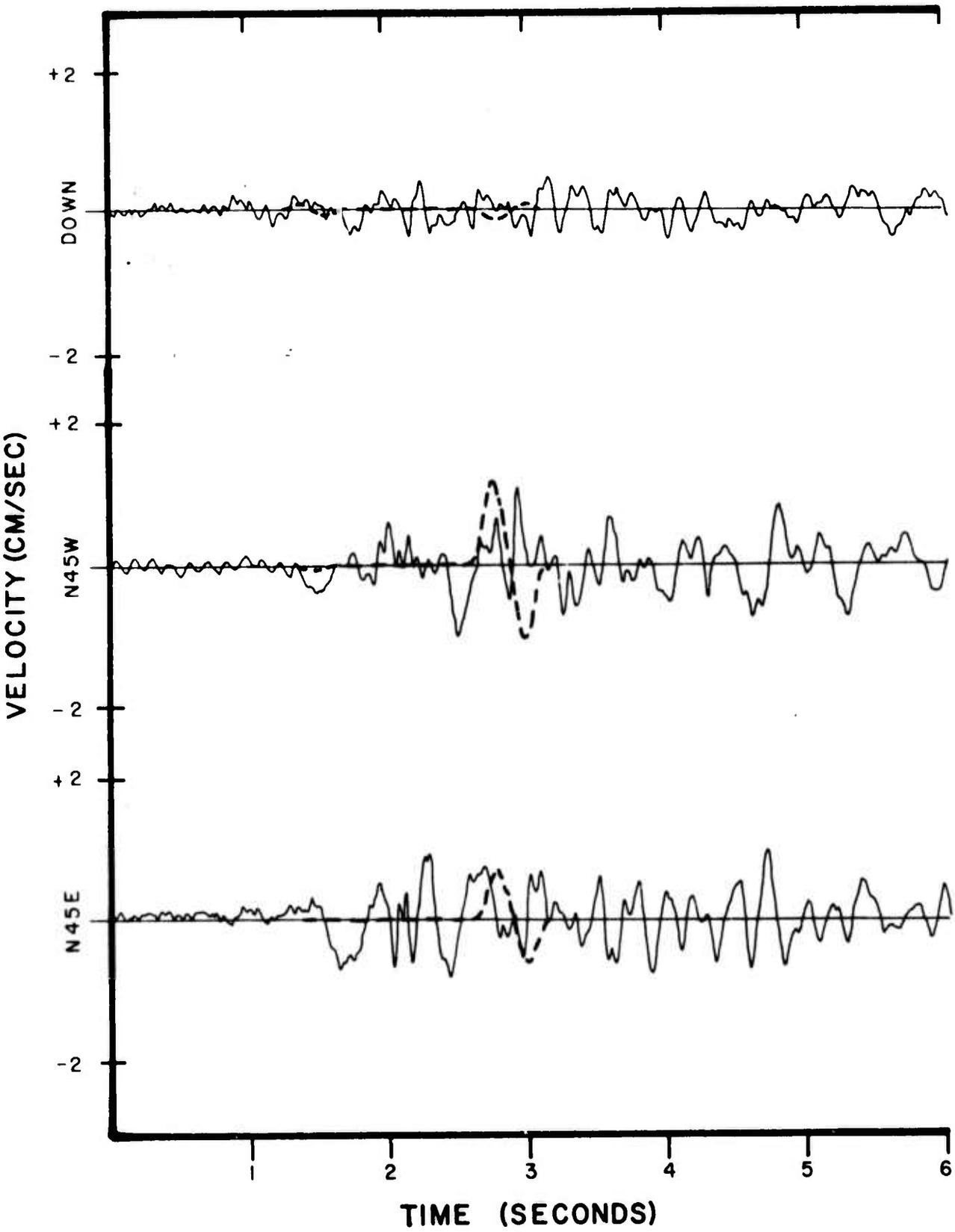


FIGURE IV-3b

OBSERVED (SOLID CURVE) AND THEORETICAL (DASHED CURVE) VELOCITY TRACE FOR RESTRICTED SOLUTION OF BEAR VALLEY EARTHQUAKE AT EPICENTER E-2, SITE 2

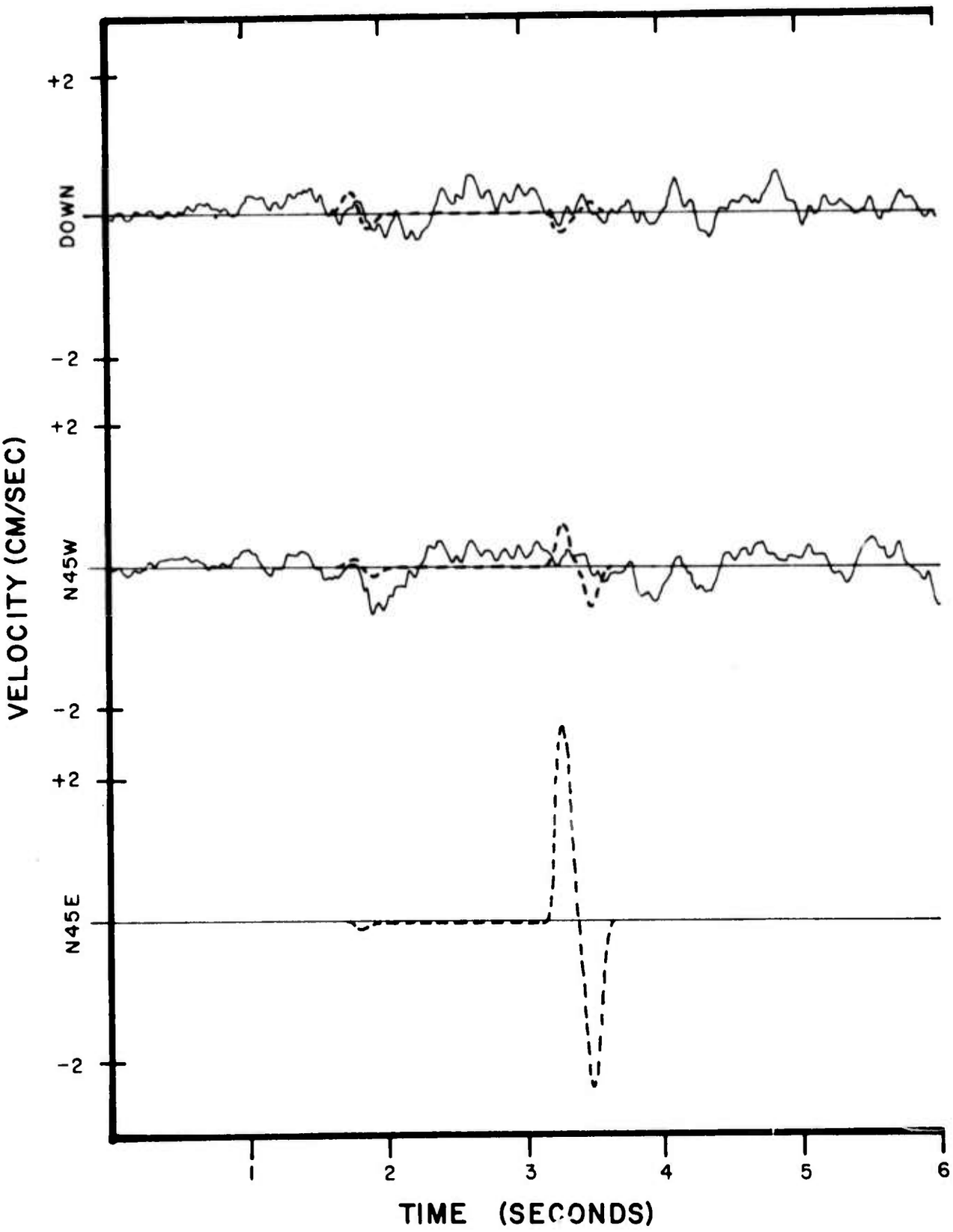


FIGURE IV-3c

OBSERVED (SOLID CURVE) AND THEORETICAL (DASHED CURVE) VELOCITY TRACE FOR RESTRICTED SOLUTION OF BEAR VALLEY EARTHQUAKE AT EPICENTER E-2, SITE 4

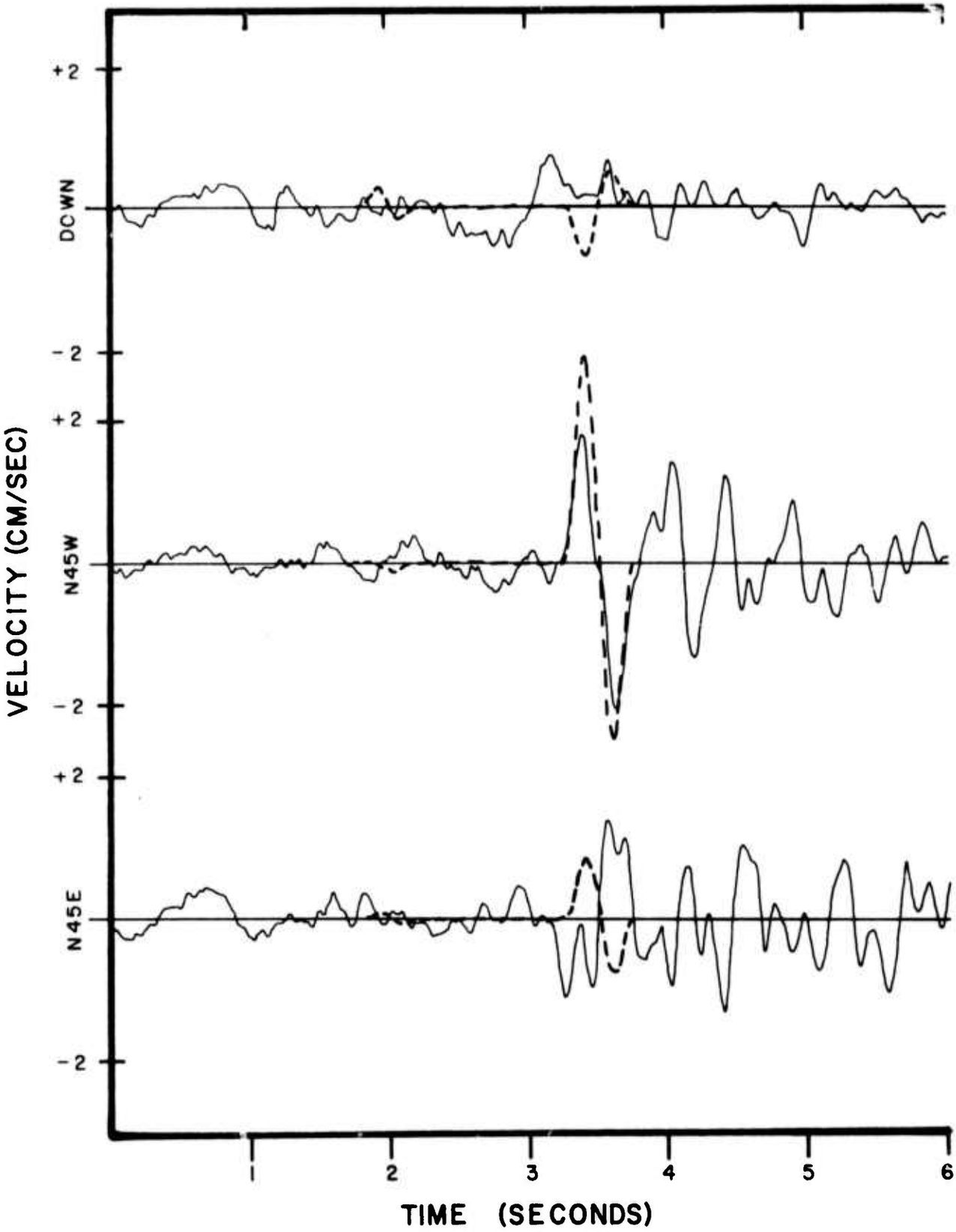


FIGURE IV-3d

OBSERVED (SOLID CURVE) AND THEORETICAL (DASHED CURVE) VELOCITY TRACE FOR RESTRICTED SOLUTION OF BEAR VALLEY EARTHQUAKE AT EPICENTER E-2, SITE 7

the empirical velocity waves by aligning the apparent P-wave arrivals. The theoretical results at Station 7 are significantly in disagreement with the empirical results. With the restrictions of the fault plane solution, the amplitude of the N45$^{o}$W component and the polarity of the S-wave on the N45$^{o}$W component can not be matched while still fitting Station 8. It can only be assumed that the geologic structure between the epicenter and either Station 7 or 8 has distorted the signals sufficiently such that it is unreasonable to expect a fit at both stations. Since Station 8 seems to have the cleaner signal, it is assumed that the signal at site 7 is the distorted signal.

The unrestricted solution (Figure IV-4) seems to do a better overall job in reproducing the velocity traces. The fit at Stations 2, 4, and 8 (Figures IV-4a, IV-4b, IV-4c) are very similar to the restricted results. However, by allowing the dip to be directed to the southwest rather than northeast, the apparent polarity and amplitude of the S-arrival at Station 7 (Figure IV-d) is matched better than in the previous solutions.

Besides the difference in dip angles between the restricted and unrestricted solutions, an important difference exists in the dislocation amplitudes. McEvilly and Johnson (1973), doing spectral analysis of the Bear Valley records and using Brune's far-field model as an approximation of the near-field, obtained a seismic moment for this earthquake of approximately $10^{23}$ dyne-cm, based on Stations 7 and 8. Using the fault area found with the Haskell model, this indicates a total dislocation of about 140 cm. This value is also substantiated by spectral analysis by Hanks (personal communication) and waveform fitting by Trifunac (personal communication) using different sources of data. We have also carried out spectral analysis of the accelerogram data and obtained a similar dislocation amplitude.

When the value of 100 cm total dislocation is compared to the dislocations required by each solution, it becomes apparent that the

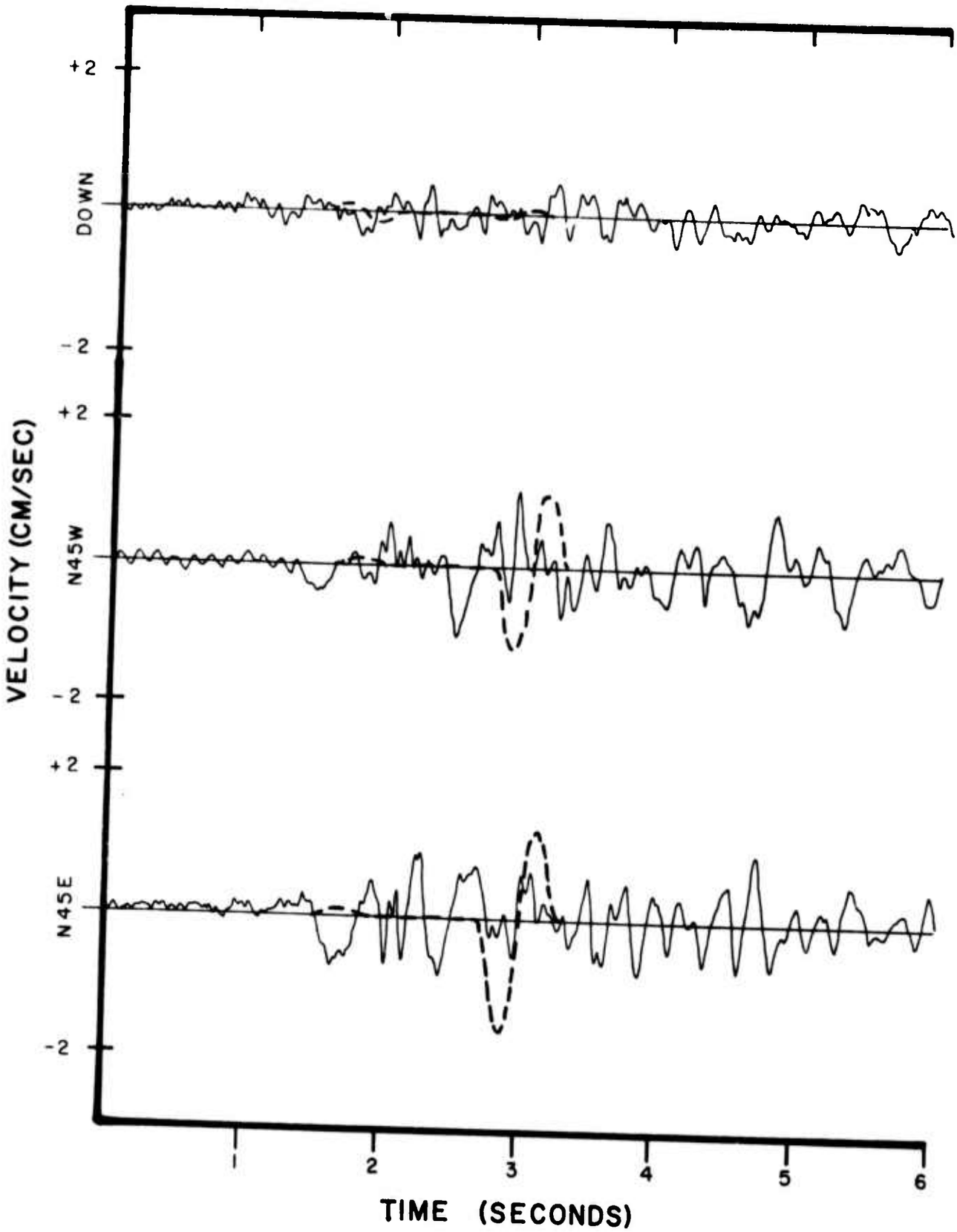


FIGURE IV-4a

OBSERVED (SOLID CURVE) AND THEORETICAL (DASHED CURVE) VELOCITY TRACE FOR UNRESTRICTED SOLUTION OF BEAR VALLEY EARTHQUAKE AT EPICENTER E-1, SITE 2

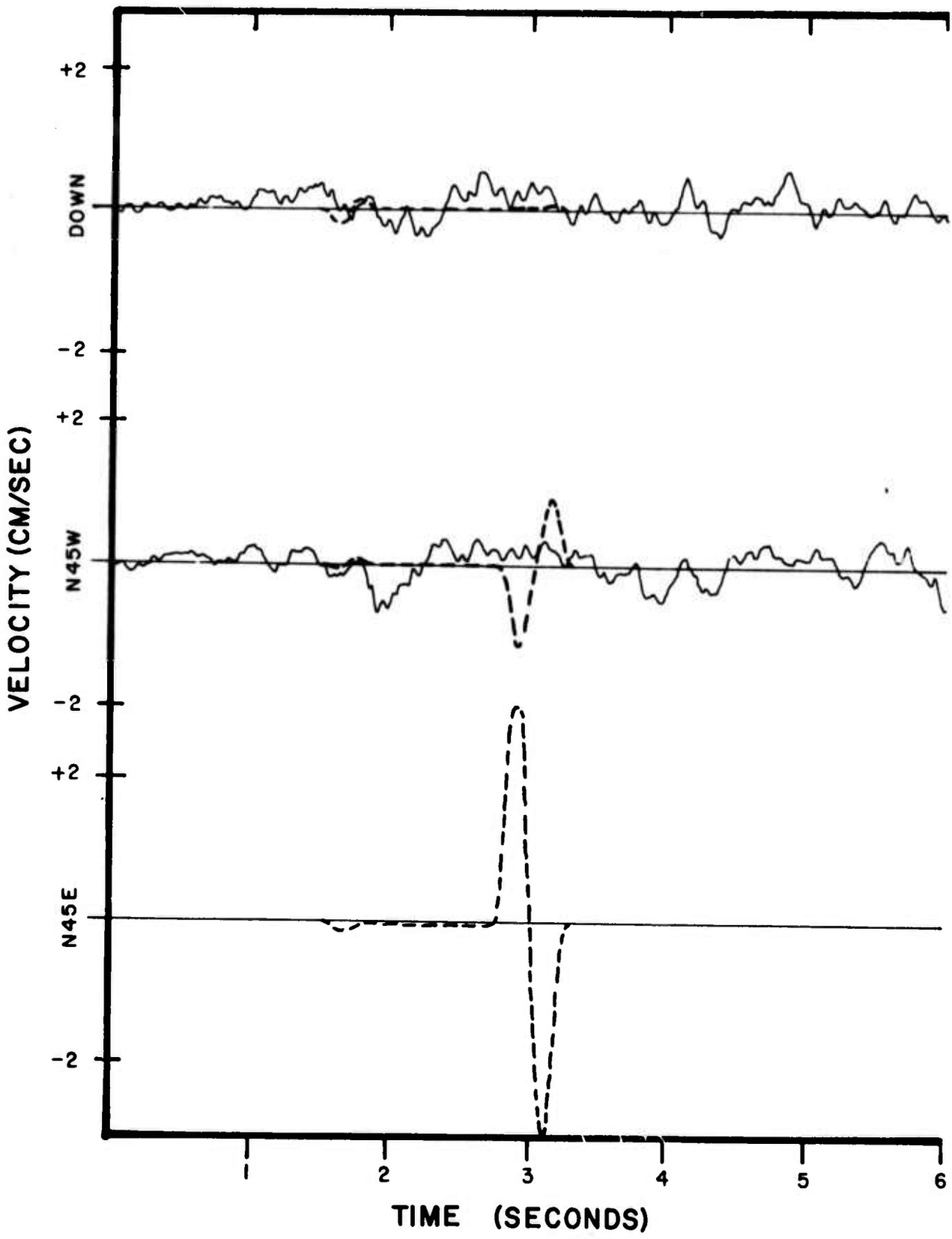


FIGURE IV-4b

OBSERVED (SOLID CURVE) AND THEORETICAL (DASHED CURVE) VELOCITY TRACE FOR UNRESTRICTED SOLUTION OF BEAR VALLEY EARTHQUAKE AT EPICENTER E-1, SITE 4

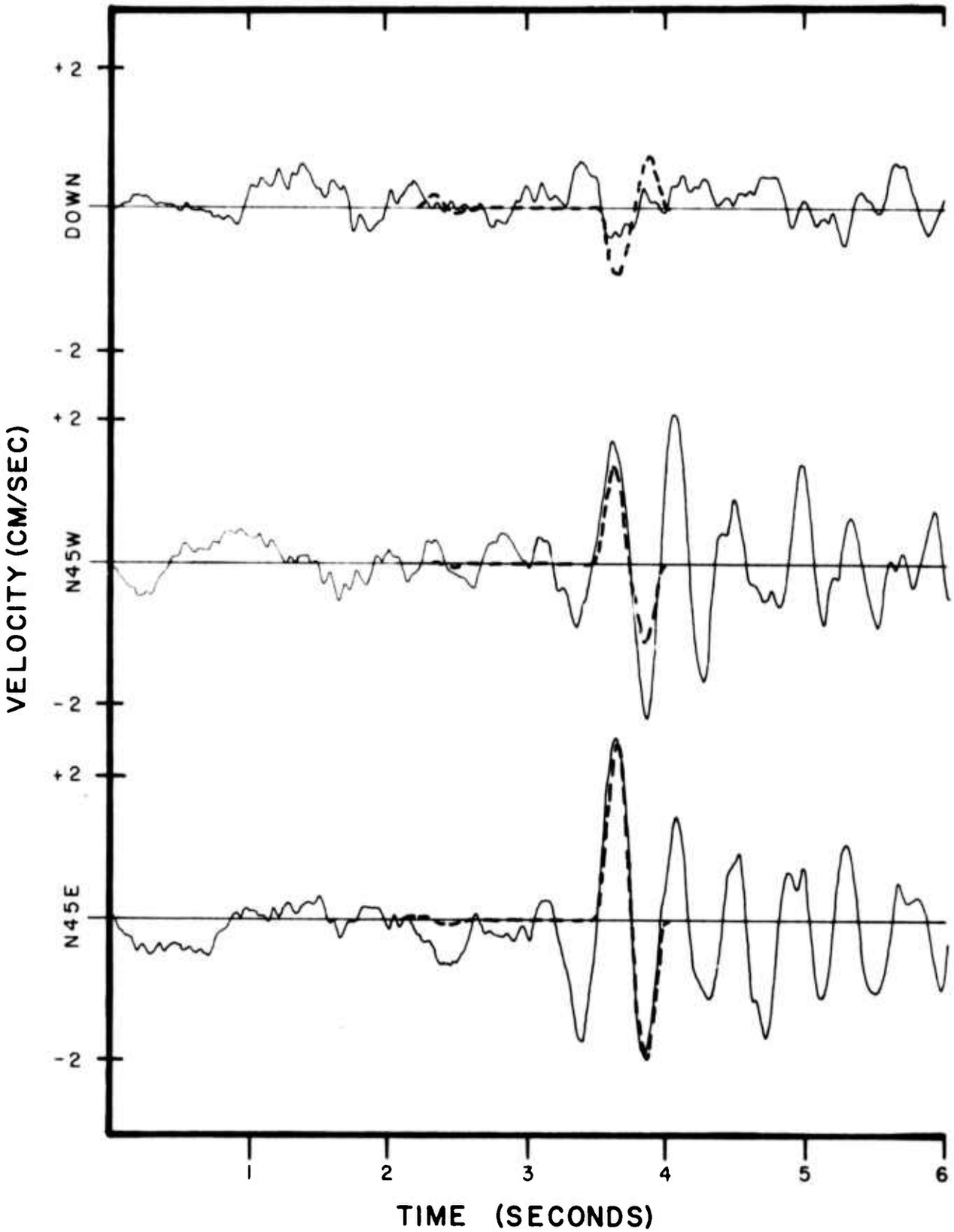


FIGURE IV-4c

OBSERVED (SOLID CURVE) AND THEORETICAL (DASHED CURVE) VELOCITY TRACE FOR UNRESTRICTED SOLUTION OF BEAR VALLEY EARTHQUAKE AT EPICENTER E-1, SITE 8

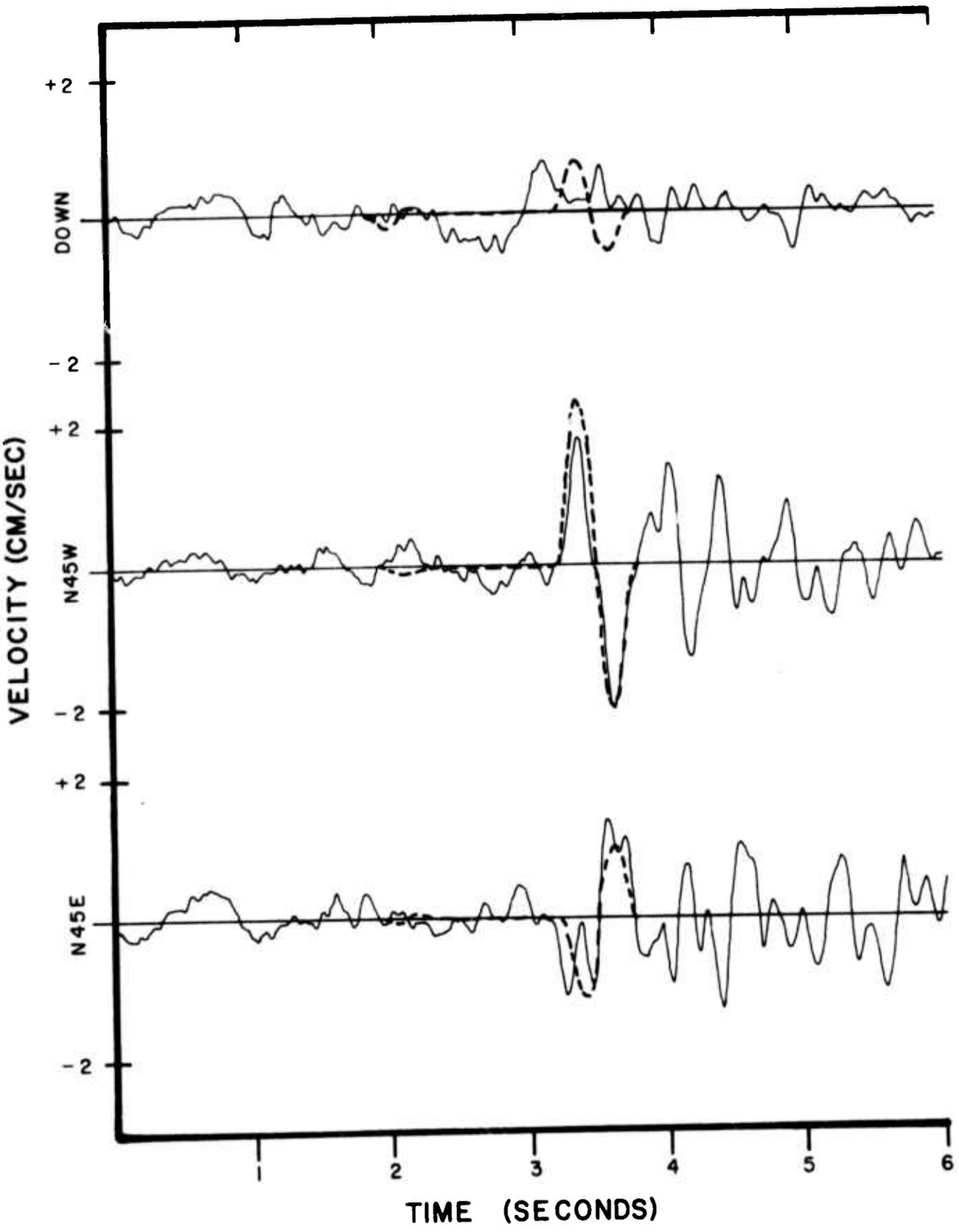


FIGURE IV-4d

OBSERVED (SOLID CURVE) AND THEORETICAL (DASHED CURVE) VELOCITY TRACE FOR UNRESTRICTED SOLUTION OF BEAR VALLEY EARTHQUAKE AT EPICENTER E-1, SITE 7

unrestricted solution is considerably out of line with information concerning this event. Not only is the orientation of the dip angle greatly different from that of the fault plane solution, but the total dislocation of 250 cm is well above any other estimates. It is immediately apparent that a Haskell model solution obtained without collaborative evidence must be considered suspect.

Little distinction can be made, however, between the two restricted solutions. Each satisfies the fault plane solution, and each does an equal job in fitting the waveforms. The total dislocations are also very close; the solution at E-1 having a total dislocation of 109 cm while the one at E-2 is 100 cm. The inherent non-uniqueness of the Haskell model enables the finding of reasonable solutions at the two epicenters. The only distinctions between the two source models are the epicenters and the necessity for dip-slip dislocation at epicenter E-1.

## B. SPECTRAL ANALYSIS OF THE BEAR VALLEY ACCELEROGRAM DATA

In addition to source models, such as Haskell's moving dislocation model, which use waveform fitting as a method of determining earthquake source characteristics, other models have been proposed which approach the problem through spectral analysis. The most widely used of this type of model is that of Brune (1970). In order to determine the correlation between the source characteristics of a frequency domain and time domain model, a program to perform spectral analysis of the Bear Valley earthquake accelerograms was implemented.

The FORTRAN computer program RENO, for which a simplified flow chart is given in Figures IV-5a, IV-5b, was designed to handle the raw accelerogram data in the same manner as the program which was utilized in plotting the accelerograms for use in waveform fitting. This was done to ensure that the signals which were processed by both techniques would be

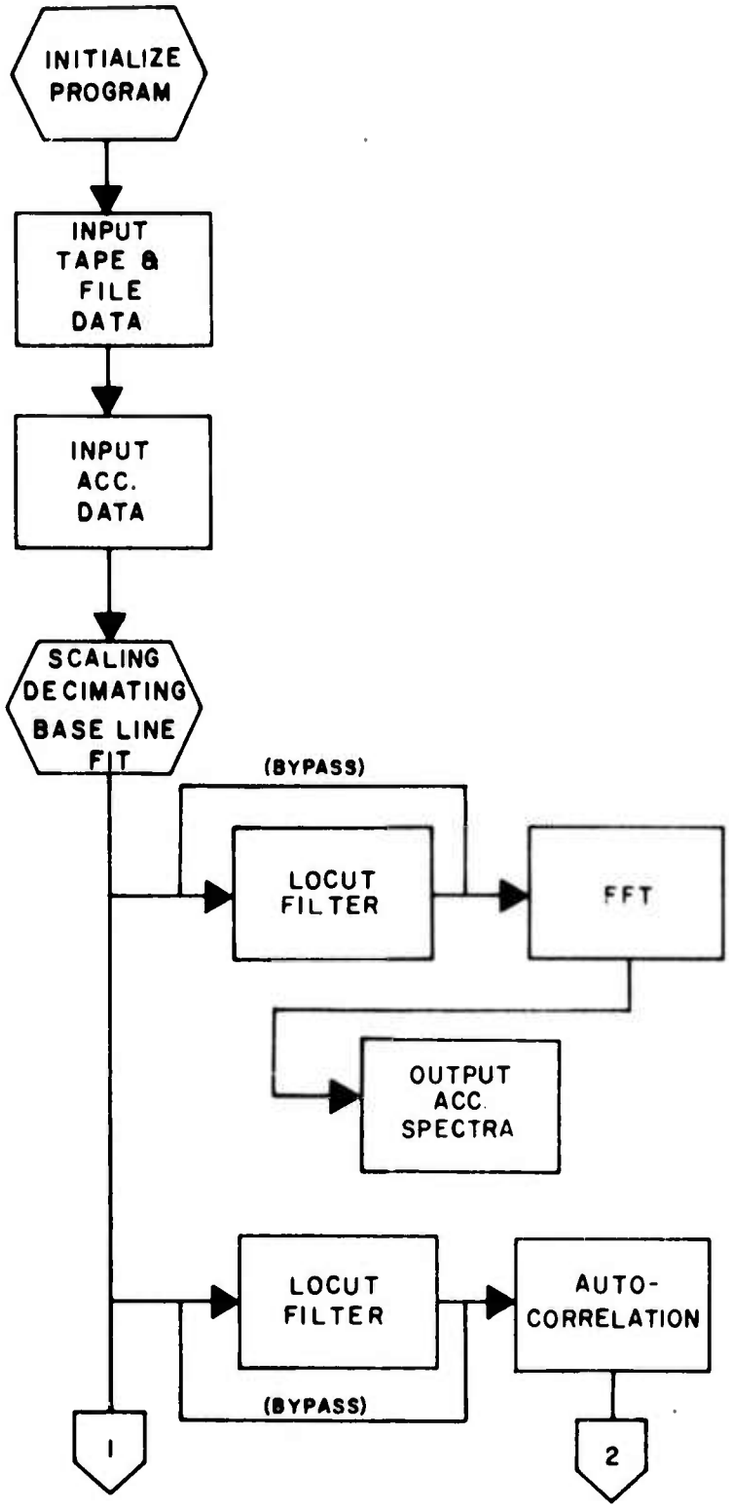


FIGURE IV-5a

SIMPLIFIED FLOW CHART OF SPECTRAL ANALYSIS PROGRAM RENO

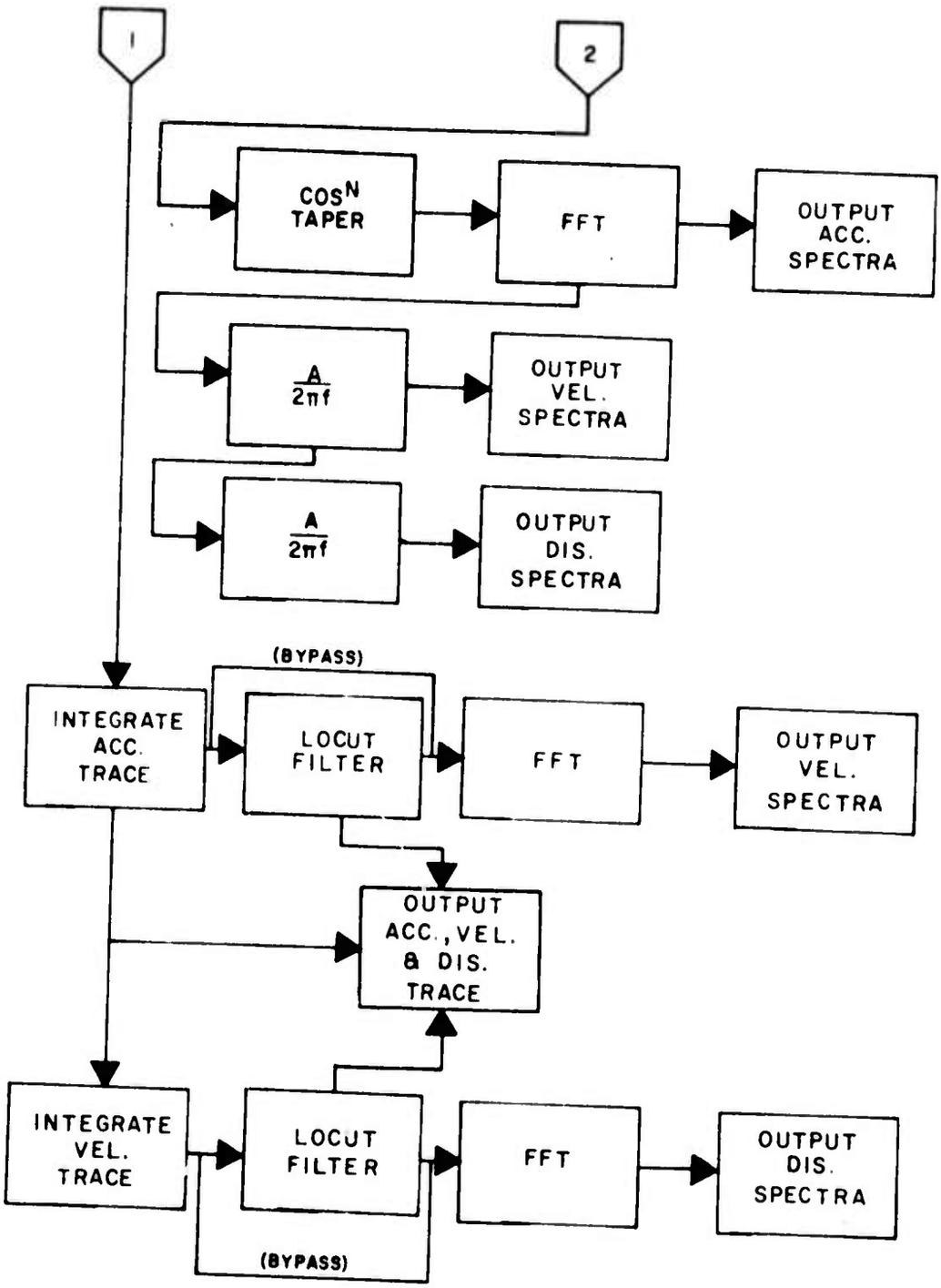


FIGURE IV-5b

SIMPLIFIED FLOW CHART OF SPECTRAL ANALYSIS PROGRAM RENO

identical. This similarity of analysis was carried out through the high-pass filtering (LOCUT).

Frequency domain models require knowledge of the displacement energy density spectra of the desired earthquake. Two distinct methods were employed to obtain this spectra. In the first method, the raw acceleration trace was numerically integrated twice to produce a displacement trace on which, after high-pass filtering, Fourier analysis was applied and the displacement energy density spectra was constructed. The second method used the same acceleration trace, but an autocorrelation function was calculated. To eliminate contaminating noise, the signal was high-pass filtered prior to obtaining the autocorrelation function. A $(\text{cosine})^N$ taper was then applied to the autocorrelation function before calculating the amplitude spectra. The displacement energy density spectra is then calculated by two divisions of the amplitude spectra by $2\pi f$.

In addition to calculating the desired displacement spectra, the program also displayed the acceleration and velocity energy density spectra for each method, and the acceleration, integrated velocity, and displacement traces. By comparison of the various energy density spectra, it became apparent that numerical integration introduced large errors in the displacement energy density spectra, and only the autocorrelation spectra were used in the final analysis.

Normalized energy density spectra for the N45$^{\circ}$E component of the accelerogram record of the Bear Valley Earthquake at Station 8 are shown in Figures IV-6 through IV-9 as examples of the output of this computer program. From comparison of the raw acceleration energy density spectra (Figure IV-6) and the autocorrelation equivalent (Figure IV-7), it can be seen that the latter gives a smoother estimate of the spectra without losing any significant detail.

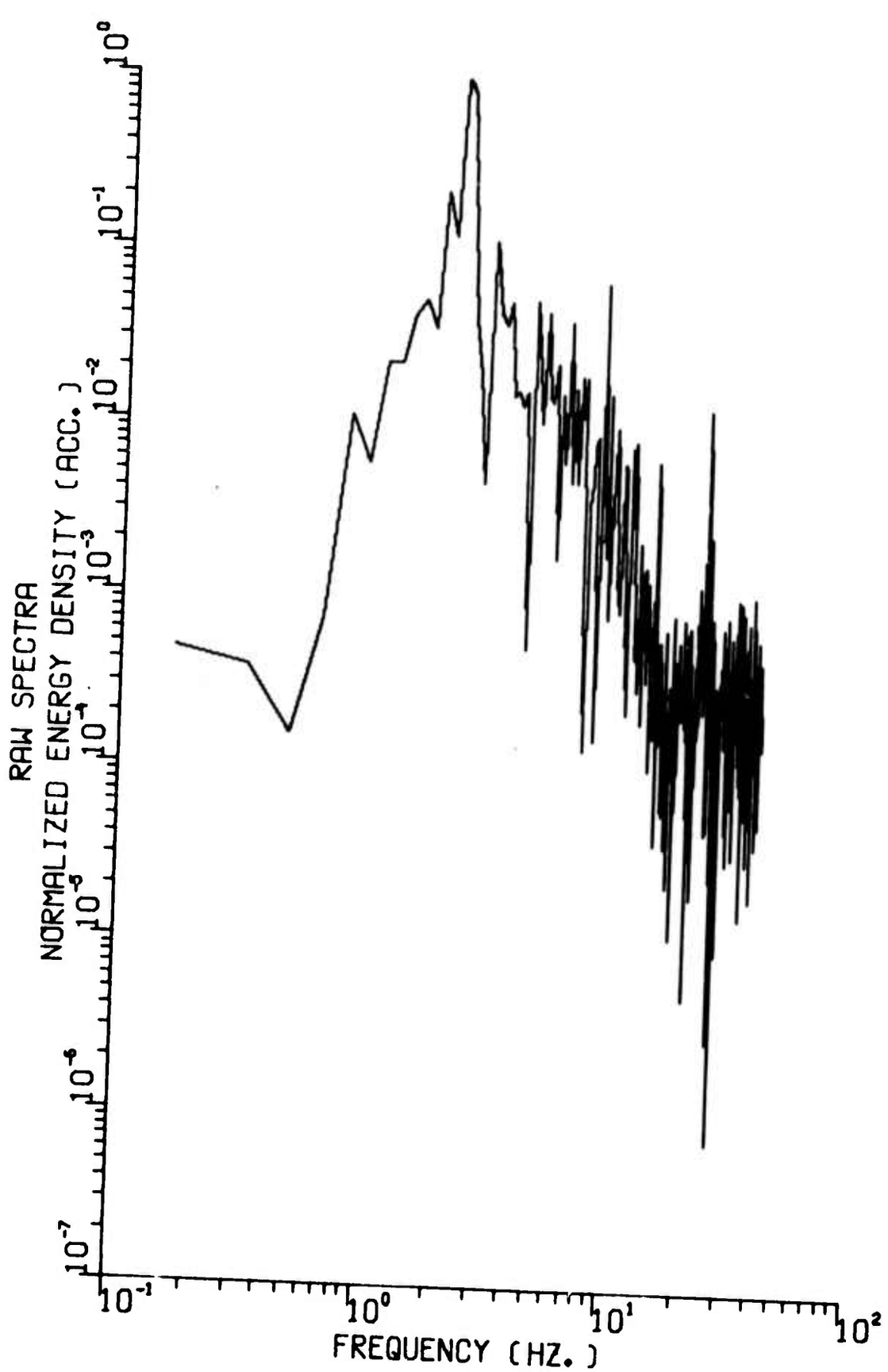


FIGURE IV-6

NORMALIZED ACCELERATION ENERGY DENSITY SPECTRUM FOR N45°E COMPONENT OF STATION 8; BEAR VALLEY EARTHQUAKE

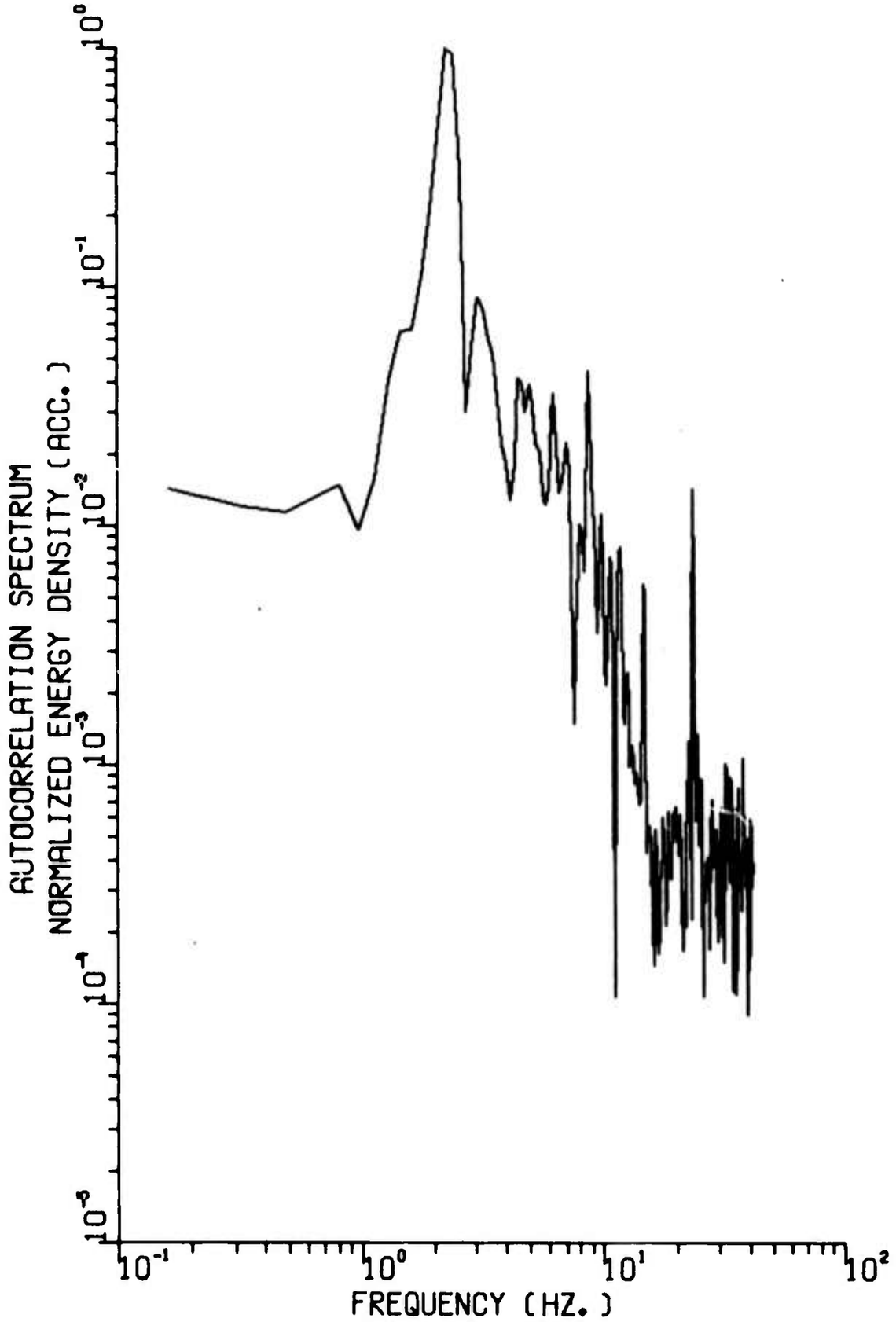


FIGURE IV-7

NORMALIZED ACCELERATION AUTOCORRELATION SPECTRUM FOR N45°E COMPONENT OF STATION 8; BEAR VALLEY EARTHQUAKE

A pronounced peak occurs in the velocity spectra (Figure IV-8) at a frequency of 2.3 Hz. This peak corresponds to the corner frequency, $f_o$, of the energy density spectra of the displacement trace (Figure IV-9). Using the spectra of Station 7, an equivalent peak is found at 2.1 Hz. Using Brune's model, with the assumption that the far-field equations can be utilized to approximate the near-field, then

$$r = \left(\frac{7\pi}{4}\right)^{1/2} \quad \frac{\beta}{2\pi f_o} \tag{IV-1}$$

where $\beta$ is the S-wave velocity and r is the radius of a circular dislocation used to model the spectrum. Strictly, this equation holds only for the S-wave spectra. In the case of the P-wave spectra, $\alpha$, the P-wave velocity would replace $\beta$. In our case, both phases were used in the calculation of the spectra. However, as the S-wave is by far the predominent phase, $\beta$ is used in these equations. Using this equation a maximum fault radius of 0.57 km is found. The fault area for this radius is 1.0 $km^2$, which is much larger than the fault area determined by Haskell's model (0.375 $km^2$).

The Haskell model area can be converted to an equivalent circular dislocation radius, using the formula

$$r = \left(\frac{A}{\pi}\right)^{1/2} \tag{IV-2}$$

where A is the fault area. Then, the radius, r, is 0.35 km. Using equation (IV-1), this would imply a corner frequency of approximately 3.5 Hz. Both Hanks, and Johnson and McEvilly (personal communications, 1974), have suggested that high frequency attenuation has effected the shape of the Bear Valley earthquake spectra. If this is true, then the corner frequency from the spectra can only be considered an upper limit. This would imply a small fault area, as found from the Haskell model, to be reasonable for this event.

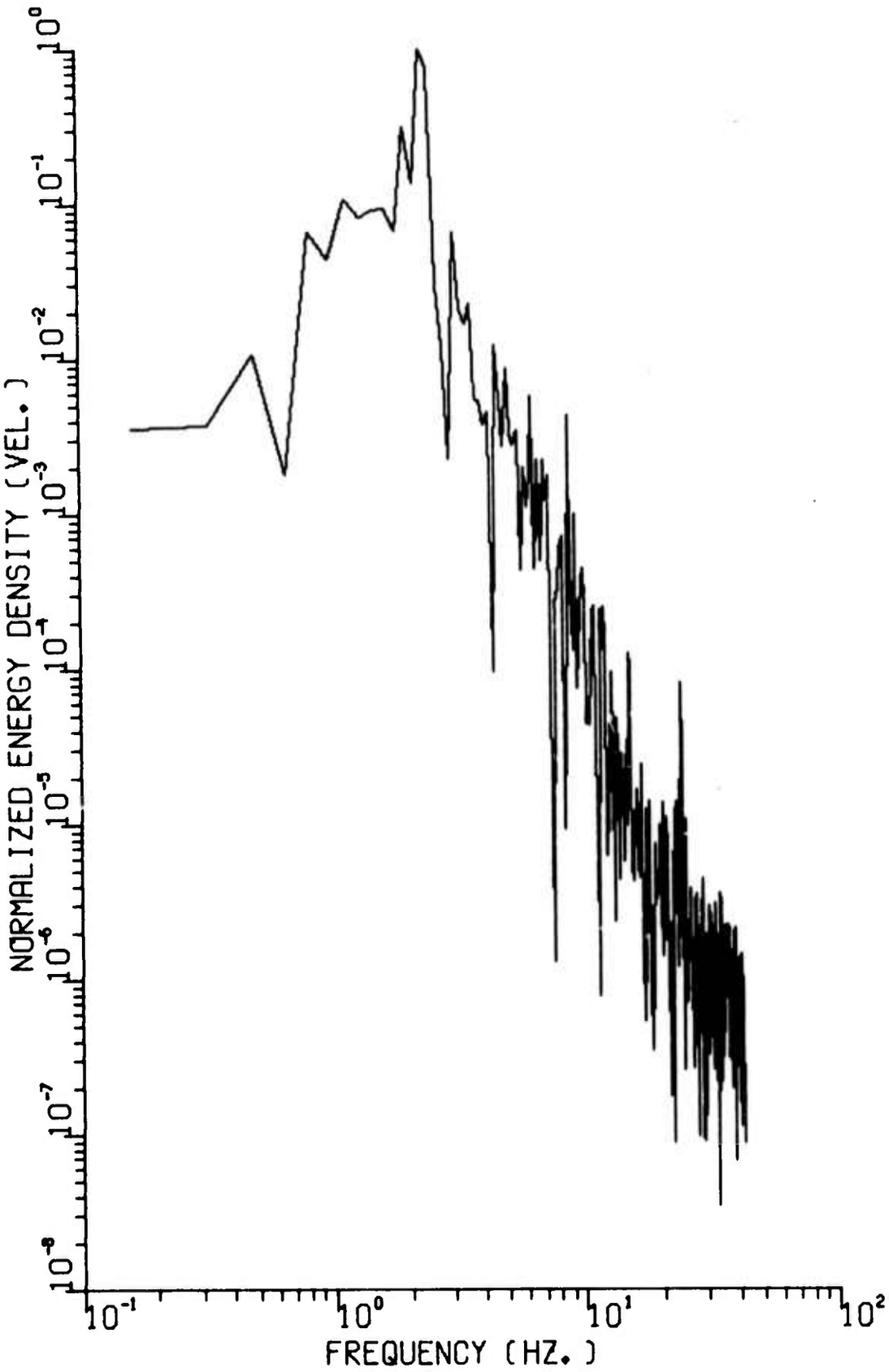


FIGURE IV-8

NORMALIZED VELOCITY ENERGY DENSITY SPECTRUM FOR N45°E COMPONENT OF STATION 8; BEAR VALLEY EARTHQUAKE

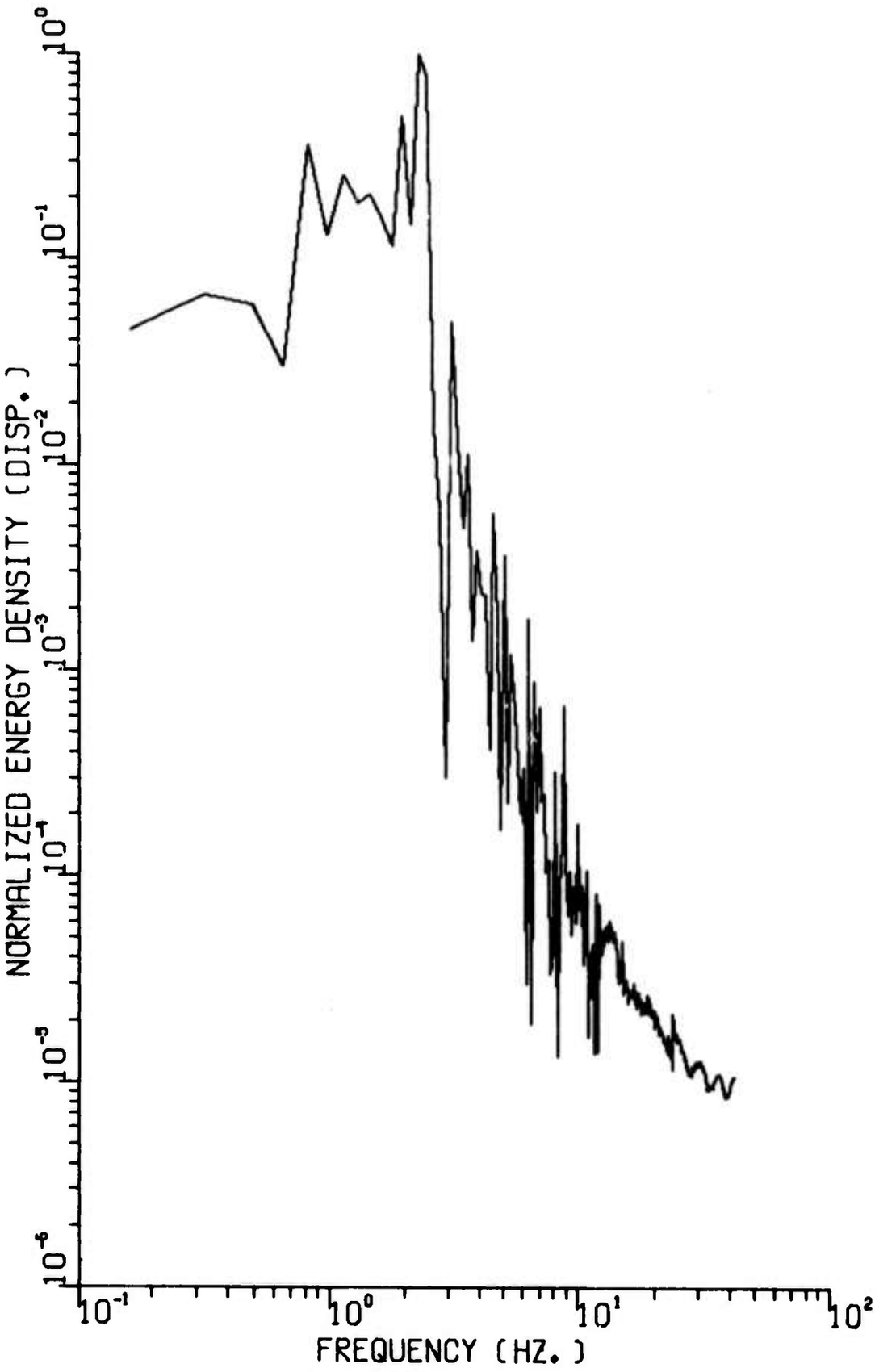


FIGURE IV-9

NORMALIZED DISPLACEMENT ENERGY DENSITY SPECTRUM FOR N45°E COMPONENT OF STATION 8; BEAR VALLEY EARTHQUAKE

An estimation of the total dislocation of the Bear Valley earthquake can be obtained from the low-frequency level of the displacement spectra. In Figure IV-9 (the displacement energy density spectra for the N45$^{o}$E component at Station 8), the spectrum is essentially flat between approximately 1 Hz, just above the corner frequency of the high-pass filter applied to the data, and 2.3 Hz, the apparent corner frequency of the earthquake spectra. Over this region, and an equivalent region on the spectra of Station 7, a simple average of the spectral level was obtained.

Again assuming that the Brune far-field model is an adequate approximation of the near-field spectra, then the seismic moment, $M_o$, of an earthquake is given by

$$M_o = 4\pi\rho\beta^3 R\,\Omega_o \qquad \text{(IV-3)}$$

where $\rho$ is the density, $\beta$ the S-wave velocity, R is the source to receiver distance and $\Omega_o$ the low frequency level. In terms of the dislocation, the moment is given by

$$M_o = \mu AD \qquad \text{(IV-4)}$$

where A is the fault area, $\mu$ the rigidity, and D is the total dislocation. Using the area determined by the Haskell model, and an assumed value for $\mu$, then the total dislocation can be calculated. This procedure was carried out, and the values used with the results are given in Table IV-4.

The values of the low frequency level which were obtained through this analysis are different, than those which were calculated by Mc Evilly and Johnson (1973). It is believed some of these discrepancies result from differences in how the data was processed. If the values given by Mc Evilly and Johnson are resolved, virtually identical moments and dislocations

TABLE IV-4

SPECTRAL LEVELS AND DISLOCATIONS OF THE BEAR VALLEY EARTHQUAKE

$\Omega_o$ - Low Frequency Levels

| | N45E | N45W | Down | Resolved | |
|---|---|---|---|---|---|
| Station 8 | 0.0962 | 0.092 | 0.0199 | 0.135 | (cm-sec) |
| Station 7 | 0.0804 | 0.0998 | 0.036 | 0.133 | (cm-sec) |

$M_o$ - Spectral Seismic Moments

$$M_o = 4\pi\rho\beta^3 R\,\Omega_o$$

$\rho$ = 2.67 gm/cm$^3$

$\beta$ = 3.2 km/sec

R = 10.1 km for Station 8

R = 11.0 km for Station 7

| | Station 8 | Station 7 | Average | |
|---|---|---|---|---|
| $M_o$ | $1.5 \times 10^{23}$ | $1.6 \times 10^{23}$ | $1.55 \times 10^{23}$ | (dyne-cm) |

D - Implied Dislocation

$$D = M_o/\mu A$$

$\mu = 3 \times 10^{11}$ dyne/cm$^2$

A = 0.375 km$^2$

| | Station 8 | Station 7 | Average | |
|---|---|---|---|---|
| D | 133 | 142 | 138 | (cm) |

are found, with an average seismic moment for Stations 7 and 8 of $1.45 \times 10^{23}$ dyne-cm.

Essentially the spectral analysis is seen to substantiate the salient features of the source model for the Bear Valley Earthquake determined by the Haskell dislocation model. Both appear to require a large dislocation, of the order of 100 cm, over a small fault area, less than 1.0 $km^2$.

# SECTION V
# CONCLUSIONS

Haskell's moving dislocation source model has been applied in the interpretation of near-field strong-motion earthquake records. Using simple planar source geometry, source mechanism solutions were obtained for the San Fernando earthquake of February 9, 1971, its first aftershock, the Parkfield earthquake of June 28, 1966, and the Borrego Mountain earthquake of April 9, 1968. It was found that a linear ramp dislocation source-time function appears to be superior to an exponential ramp function for interpreting these strong motion records. Because Haskell's source is formulated in a whole space, valid matching of waveforms can only be accomplished for records within a few kilometers of the fault trace. Further, a dislocation model with a finite rupture velocity was found to be required to explain near-field velocity waveforms from an event with significant fault dimensions (approximately 10 km).

Upon generalizing the Haskell model to include fault segments having their own rupture velocities, dislocations, and dimensions, the effect of stick-slip alone (segmented rupture velocities) was found to be minor within a moderate range of rupture velocities. Having two segments with different dip angles (a hinged fault surface), though, produce significant changes. The San Fernando main shock was re-examined with such a fault surface, and the improved fit on all components was quite noticeable.

With the corrected orientation of the Pacoima Dam instruments, a reasonable match to the observed waveforms of this event could only be accomplished by having a large strike-slip component on the lower element of

the fault. Three small aftershocks of the San Fernando event were also re-analyzed with the new orientation. Two of these events were located in the same place as determined by Trifunac (1972), while the third, event 30, was found to lie in a different location. Because of the small source size of these aftershocks, and the lack of independent estimates of the fault parameters, our solutions can be considered the best possible within the limitations of the model.

Another small event, the Bear Valley earthquake of June 22, 1973, was examined using both Haskell's model and spectral analysis. Independent estimates of the source orientation and depth were available from first motion studies. Both approaches yielded substantially the same results; a large dislocation on the order of 100 cm over a small fault area of less than 1.0 $km^2$, with a seismic moment of 1.2 to 1.5 x $10^{25}$ dyne-cm.

Finally, in Figure V-1, the logarithm of the seismic moment is plotted as a function of Wood-Anderson local magnitude ($M_L$) for the eight events discussed above, as determined by the Haskell model and by other authors. Most of the differences in values can be explained by lack of independent estimates of the fault parameters (events 30 and 4), the uncertainty of the fault length of the Parkfield earthquake, and the uncertainty of the fault width of the Borrego Mountain event. From the distribution of all values, one could possibly assume a linear log magnitude-moment relation for these points, except for the value for the Bear Valley earthquake determined by the Haskell model. When other estimates are obtained for this event, we will be able to judge whether other factors, such as site amplification, should be included in our analysis, or that this event is an exception to the observed trend.

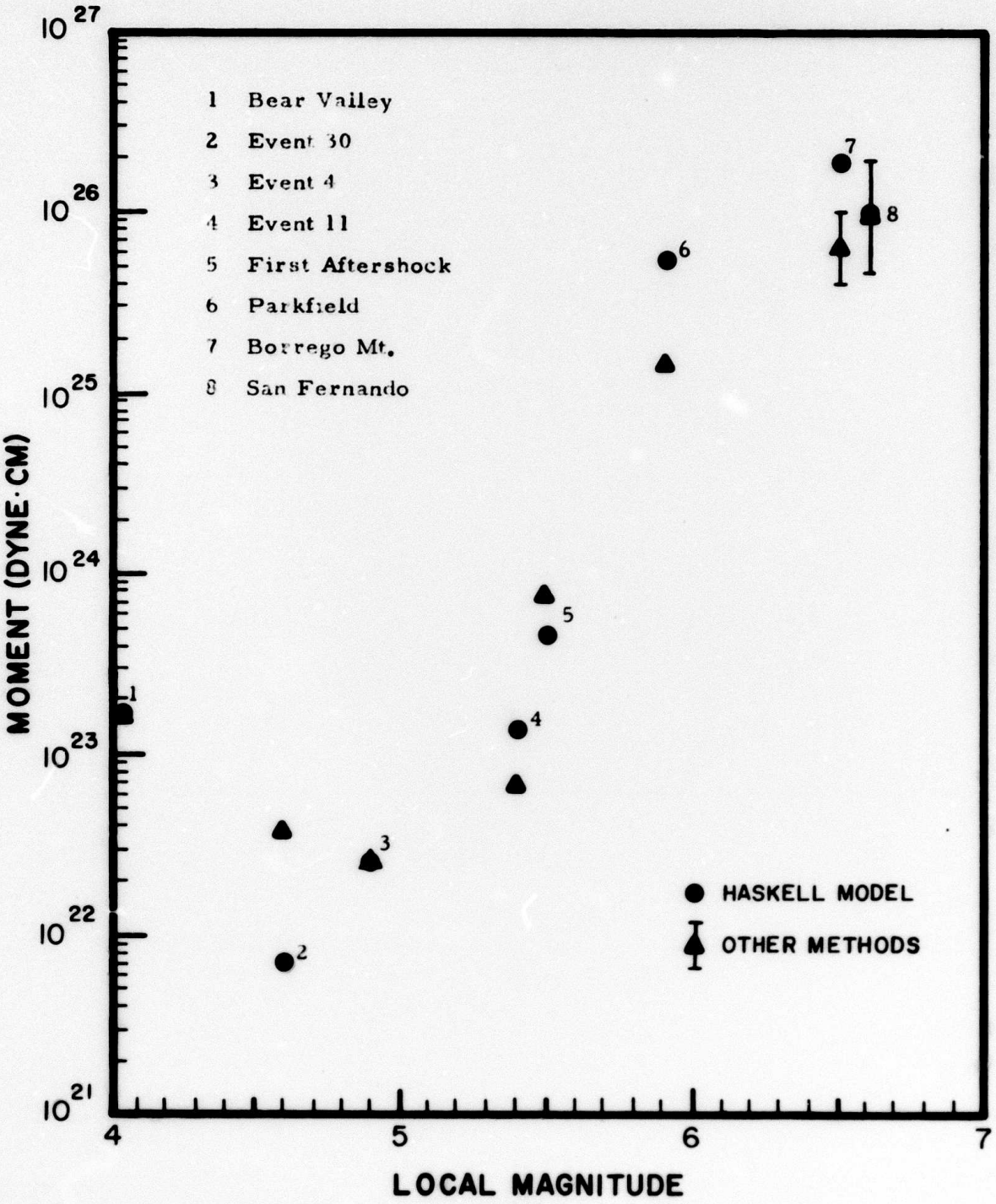


**FIGURE V-1**

**SEISMIC MOMENTS FOR EIGHT ANALYZED EVENTS VERSUS LOCAL MAGNITUDE ($M_L$)**

# SECTION VI
# REFERENCES


Alewine, R. W., 1974, Application of Linear Inversion Theory Toward the Estimation of Seismic Source Parameters, Ph. D. Thesis, California Institute of Technology, Ch. 4.

Brune, J. N., 1970, Tectonic Stress and the Spectra of Seismic Shear Waves, J. Geophysical Research, 75, 4997-5009.

Canitez, N., and M. N. Toksoz, 1972, Static and Dynamic Study of Earthquake Source Mechanism: San Fernando Earthquake, J. Geophysical Research, 77, 2583-2594.

Hanks, T. C., 1974, Near-Field Project Review, personal communication, Las Vegas, Nevada.

Haskell, N., 1969, Elastic Displacements in the Near-Field of a Propagating Fault, Bulletin of the Seismological Society of America, 59, 865-908.

Johnson, L. R., 1974, personal communication.

Malone, S. D., 1974, personal communication.

McEvilly, T. V., and L. R. Johnson, 1973, Near-Field Accelerometer Array, Technical Report No. 2, AFOSR Grant No. 72-2392, 2392A, University of California, Berkeley, California.

Trifunac, M. D., 1972, Stress Estimates for the San Fernando, California Earthquake of February 9, 1971: Main Event and Thirteen Aftershocks, Bulletin of the Seismological Society of America, 62, 721-750.

Trifunac, M. D., 1974, Near-Field Project Review, personal communication, Las Vegas, Nevada.

Tsai, Y. B., and H. J. Patton, 1972, Near-Field Small Earthquakes - Dislocation Motion, Semi-Annual Technical Report No. 1, AFOSR Contract No. F44620-72-C-0073, Texas Instruments Incorporated, Dallas, Texas.

Tsai, Y. B., and H. J. Patton, 1973, Dislocation Motion and Theoretical Far-Field Source Spectra of Four California Earthquakes, Semi-Annual Technical Report No. 2, AFOSR Contract No. F44620-72-C-0073, Texas Instruments Incorporated, Dallas, Texas.

Turnbull, Jr., L. S., and J. C. Battis, 1973, Interpretation of Strong-Motion Earthquake Accelerograms Using A Moving Dislocation Model, Semi-Annual Technical Report No. 3, AFOSR Contract No. F44620-72-C-0073, Texas Instruments Incorporated, Dallas, Texas.

# APPENDIX A

## A DISCUSSION OF FAULT PARAMETER VARIATION WITHIN HASKELL'S MODEL

A concise description of the equations derived by Haskell (1969) for computing the theoretical waveforms is given by Tsai and Patton (1973). They also discuss the technique adopted for numerically integrating the Green's function integrals. Briefly, the fault plane area is assumed to be rectangular with length $L$ in the $X_1$ direction and width $W$ in the $X_2$ direction as indicated in Figure A-1. Over this surface the shear dislocation is described as:

$$D_i(X_1, X_2, t) = \begin{cases} 0 & t - \frac{X_1}{V} < 0 \\ \frac{D_{io}}{T}(t - X_1/V) & 0 < t - \frac{X_1}{V} < T \\ D_{io} & t - \frac{X_1}{V} > T \end{cases} \qquad \text{(A-1)}$$

where $i = 1$ and 2 for longitudinal and transverse shear dislocation respectively. This form of dislocation function implies that at $t = 0$ a fracture front is established instantaneously over a length $W$ of the $X_2$ axis. At any fixed point on the fault plane the relative displacement $D_i$ increases at constant velocity from 0 at $t = X_1/V$ to a constant final value, $D_{io}$, at $t = T + X_1/V$. Here $T$ is referred to as dislocation rise time. The dislocation parameters needed for computation are either derived from existing seismic evidence such as the fault-plane solution, the aftershock zone, etc., or varied by trial and error until the resultant waveforms are considered to agree substantially with their observed counterparts. In our study, the comparison is accomplished using velocity waveforms. Since this source model

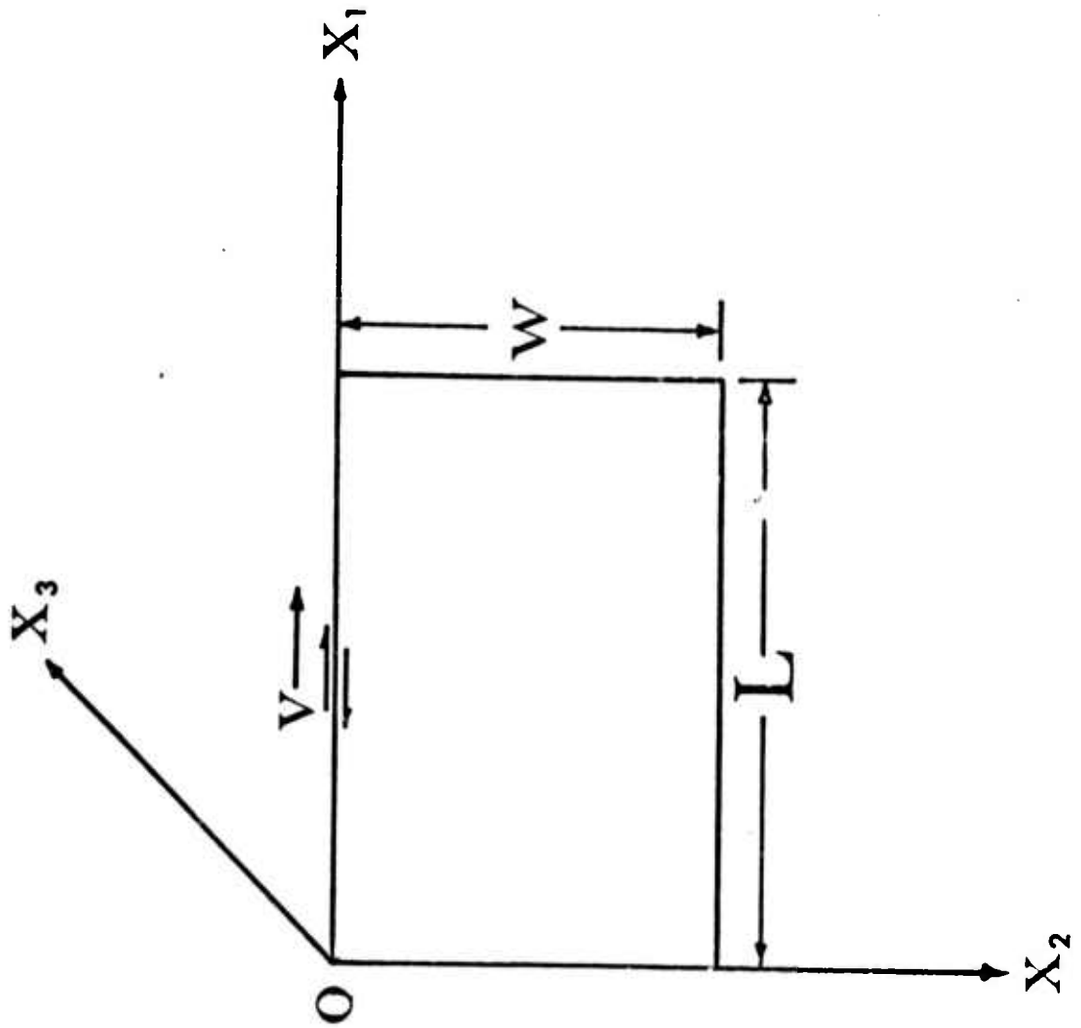


FIGURE A-1

MODEL COORDINATE SYSTEM AND
FAULT PLANE GEOMETRY

is derived for a whole space, the effect of the free surface is approximated by doubling the amplitude of the theoretical waveforms.

The model variables can be divided into two classifications. The first is what may be labeled as non-physical parameters. These are the variables which have no analog in the physical process of fault rupture. They affect the waveform only by determining the convergence of the numerical signal to the analytic solution. The second group, the physical parameters, are those which can actually determine the theoretical waveform. In the following paragraphs, we will present a rough guide of the behavior of the physical parameters.

The physical parameters include the dislocation amplitudes, rise time, rupture velocity, and fault dimensions. In addition, one must include those factors which affect the waveform in a more indirect way, specifically the orientation of the fault surface. This information is contained in the spatial position of the point of evaluation, dip angle, and azimuth. The variation of a physical parameter has extremely subtle effects due to the interrelationships of the parameters. For example, under certain conditions, it is impossible to distinguish between a variation of rise time and rupture velocity. If the position of observation is maintained, a change of the dip angle of the fault plane will rotate the observation point within the displacement field. The same effect could be obtained by holding the dip angle and altering the position of the station.

For some of the parameters, the effects of variation are seen directly from the equations of the model. For either longitudinal or transverse dislocation, the dislocation amplitude can be seen to have only a scaling effect on the waveform, with no ability to modify the form of either the displacement or velocity signal. In the case of mixed dislocation, the resulting waveform is the superposition of the waves generated by the two modes of dislocation separately. This property gives rise to the use of a least

squares technique in amplitude fitting, and yields a measure, through the residuals, of how good our fit of the theoretical to the observed waveform is.

The fault length, the linear dimension in the direction of rupture propagation, and width, the dimension transverse to the rupture, have somewhat similar effects. When one increases the fault area by altering one or both of these dimensions, one increases the source of contributors to the displacement wave. As each elemental area behaves in the same manner, one is merely adding to the amplitude in an almost linear manner. The effect is almost, but not exactly, linear due because the fault plane position is altered with respect to the observation point.

For the fault width, the added width will rupture the same instant as in the original case, but depending on where it is added, it will be either nearer or further away from the observation point. Thus, the displacements caused by this new area will arrive either earlier or later than in the original case. This alters the waveform by changing the interference pattern between contributing sources. This effect is seen mostly by a change in time durations of the waveform segments. However, the geometry of the situation and the amount of area added is exceedingly important in determining the significance of these effects.

The alteration of the fault length has similar effects to those of added fault width, but is both more complex and more significant in determining the signal duration. This results from the addition of area along the direction of rupture propagation. As with the fault width, the new area is contributing the same signal as a similar area of the original fault and it affects the resulting signal by originating at a different distance from the observation point, but it is also, due to finite rupture velocities, extending the time over which the rupture process occurs.

It should be noticed that an approximation of varying the fault length could be attained by altering rise times, rupture velocity and dislocation amplitudes.

The rise time is that period for which the dislocation at a specific point goes from zero dislocation to the final value. Obviously, this is significant in determining the time characteristics of the waveform. A fast rise time will decrease the time over which the rupture process proceeds. From the equation below,

$$T_{1(Total)} \propto L_{Fault} * 1/V_{Rupture} + T_{Rise}, \qquad (A\text{-}2)$$

The time duration of the signal is therefore reduced which alters the interference patterns producing the final wave. As the dislocation occurs quicker, the displacement amplitudes are increased.

As was previously mentioned, increasing the rupture velocity, has a similar effect to decreasing fault length. The resulting wave train is condensed in time except for the initial arrival times of the P and S waves. The effect is analogous to alteration of rise time in that the displacement amplitudes are also increased.

A significant effect resulting from the properties of the rise time, rupture velocity, and fault dimensions is the width of the P- and S-wave velocity waveforms. For some given length of the fault, rupture velocity, and rise time, a steady state displacement function will be achieved for some time period (say $T_1$). From Figure A-2 and Equation (A-1), if we double the fault length, then $T_1$ becomes significantly longer. We can also reduce $V_R$ to make $T_1$ grow. The pulse width of the velocity waveform, $T_p$, is determined by the rise time.

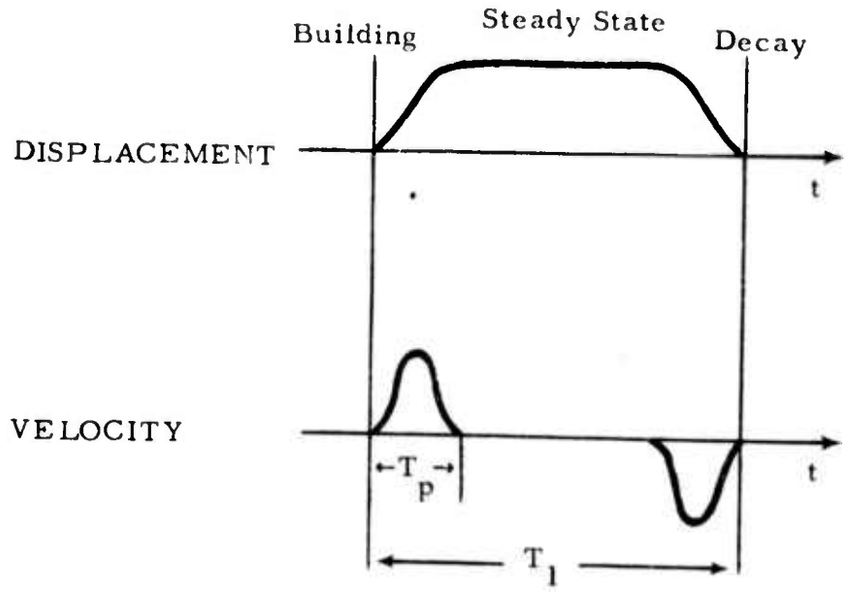


FIGURE A-2

VARIATION OF DISPLACEMENT AND VELOCITY WAVEFORMS

# APPENDIX B

## VARIATION OF THEORETICAL WAVEFORMS AS A FUNCTION OF FAULT LENGTH, FAULT WIDTH, AND RISE TIME

As presented in Section IV, our solution to the Bear Valley Earthquake of June 22, 1973 includes, among others, the following source parameters:

$$L = 0.5 \text{ km}$$
$$W = 0.75 \text{ km}$$
$$T_R = 0.1 \text{ sec}$$

The waveforms representing this 'best' solution for Station 8 is shown in Figure B-1a, 1b.

Many models were generated to obtain this solution. In the following paragraphs, some of the alternative solutions that were generated using different combinations of the above three parameters are described. Besides giving some insight into our choice of a best model, the variation of the Haskell source as a function of these parameters will be demonstrated.

- Variation of fault length only: L = 0.65, 0.75, 1.0 - In Figure B-1c, is shown the last of these cases. From the relation

$$T_{\text{Pulse Width}} \propto L/V_R + T_{\text{Rise Time}}$$

we should expect the S-wave pulse to broaden and that is exactly what happens. The amplitude change is very slight as the length varies.

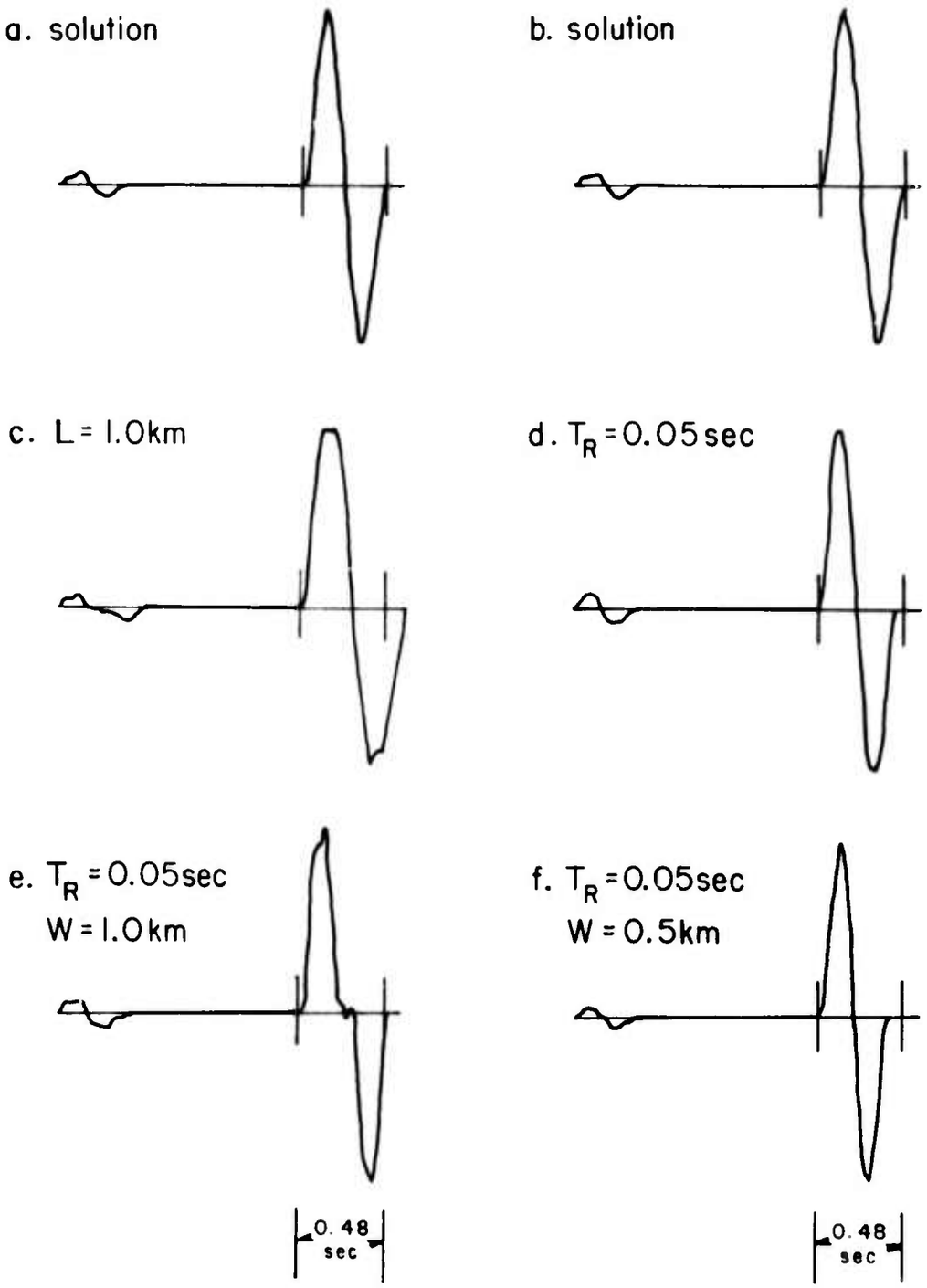


FIGURE B-1

VARIATION OF THE THEORETICAL PULSE SHAPE WITH FAULT PARAMETERS FOR THE BEAR VALLEY EARTHQUAKE OF JUNE 22, 1973

- Variation of rise time only: $T_R = 0.05$ - Shortening the rise time (see Figure B-1d) yields an S-wave pulse which is sharpened (rises to its maximum amplitude faster) with a smaller pulse width. These effects are present, but only to a slight degree, because the pulse width is also a function of the fault orientation.

- Variation of fault width and rise time: $T_R = 0.05$, $W = 0.5$, $1.0$ - Although both the rise time and fault width are varied, from the above paragraph we know that, with the 'best' solution fault orientation, the variation of the S-wave pulse was minimal. Hence, any major variation of the pulse should be due to the change in the width. Two cases are shown in Figures B-1e and B-1f, with the width 0.5 km in the former and 1.0 km in the latter. In this case, the width is varying somewhat as the fault length, with the shorter width (0.5 km) producing a sharp pulse, and the longer width (1.0 km) producing a broader pulse containing small irregularities.